Harmful Algae 116 (2022) 102254

Contents lists available at ScienceDirect

Harmful Algae

journal homepage: www.elsevier.com/locate/hal

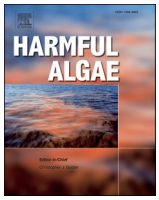

# Variability patterns and phenology of harmful phytoplankton blooms off southern Portugal: Looking for region-specific environmental drivers and predictors

M.J. Lima [a,*], P. Relvas [b], A.B. Barbosa [a]

[a] Centro de Investigação Marinha e Ambiental (CIMA), Universidade do Algarve, Campus de Gambelas, Faro 8005-139, Portugal
[b] Centro de Ciências do Mar (CCMAR), Universidade do Algarve, Campus de Gambelas, Faro 8005-139, Portugal

ARTICLE INFO

Edited by Holly Bowers

*Keywords:*
Phytoplankton phenology
Harmful algal blooms
*Pseudo-nitzschia*
*Dinophysis*
Coastal upwelling
Predictive models

ABSTRACT

Harmful algal blooms (HABs) negatively impact coastal ecosystems, fisheries, and human health, and their prediction has become imperative for effective coastal management. This study aimed to evaluate spatial-temporal variability patterns and phenology for key toxigenic phytoplankton species off southern Portugal, during a 6-year period, and identify region-specific environmental drivers and predictors. Total abundance of species responsible for amnesic shellfish poisoning (*Pseudo-nitzschia* spp.), diarrhetic shellfish poisoning (*Dinophysis* spp.), and paralytic shellfish poisoning (*G. catenatum*) were retrieved, from the National Bivalve Mollusk Monitoring System public database. Contemporaneous environmental variables were acquired from satellite remote sensing, model-derived data, and *in situ* observations, and generalized additive models (GAMs) were used to explore the functional relationships between HABs and environmental variables and identify region-specific predictors. *Pseudo-nitzschia* spp. showed a bimodal annual cycle for most coastal production areas, with spring and summer maxima, reflecting the increase in light intensity during the mixed layer shoaling stage, and the later stimulatory effects of upwelling events, with a higher bloom frequency over coastal areas subjected to stronger upwelling intensity. *Dinophysis* spp. exhibited a unimodal annual cycle, with spring/summer maxima associated with stratified conditions, that typically promote dinoflagellates. *Dinophysis* spp. blooms were delayed with respect to *Pseudo-nitzschia* spp. spring blooms, and followed by *Pseudo-nitzschia* spp. summer blooms, probably reflecting upwelling-relaxation cycles. *G. catenatum* occurred occasionally, namely in areas more influenced by river discharges, under weaker upwelling. Statistical-empirical models (GAMs) explained 7-8%, and 21−54% of the variability in *Pseudo-nitzschia* spp. and *Dinophysis* spp., respectively. Overall, a set of four easily accessible environmental variables, surface photosynthetically available radiation, mixed layer depth, sea surface temperature, and chlorophyll-a concentration, emerged as the most influential predictors. Additionally, over the coastal production areas along the south coast, river discharges exerted minor negative effects on both HAB groups. Despite evidence supporting the role of upwelling intensity as an environmental driver of *Pseudo-nitzschia* spp., it was not identified as a relevant model predictor. Future model developments, such as the inclusion of additional environmental variables, and the implementation of species- and period-specific, and hybrid modelling approaches, may further support HAB operational forecasting and managing over complex coastal domains.

## 1. Introduction

Phytoplankton are the main primary producers in marine ecosystems and play a key role in global carbon cycling (Falkowski et al., 1998; Cloern et al., 2014). Yet, some phytoplankton species can generate harmful algal blooms (HABs), events associated with multiple deleterious effects, including oxygen depletion, mortality of wild and cultured fish and invertebrates, toxin accumulation along the food web, eventually affecting human health (Anderson, 2009; see review by Shumway et al., 2018), and severe disruption of ecosystem dynamics and services (e.g., Gobler and Sunda, 2012). HABs can also lead to adverse economic and societal effects due to closure of fishery and

* Corresponding author.
*E-mail addresses:* mjlima@ualg.pt (M.J. Lima), prelvas@ualg.pt (P. Relvas), abarbosa@ualg.pt (A.B. Barbosa).

https://doi.org/10.1016/j.hal.2022.102254
Received 1 February 2022; Received in revised form 4 May 2022; Accepted 15 May 2022
Available online 25 May 2022

farming grounds, and impacts on tourism and other coastal businesses (Hoagland et al., 2002; Hoagland and Scatasta, 2006; Kudela et al., 2015; Berdalet et al., 2016; Sanseverino et al., 2016; Trainer, 2020). A generalized increase in the extension and frequency of HABs, associated with anthropogenic eutrophication, climate variability and introduction of non-native species, has been frequently referred in the literature (e.g., Anderson et al., 2012). However, a recent meta-analysis showed no empirical support for a global increase in HABs and, instead, related this widespread perception with increased monitoring effort, in tandem with emerging HAB socio-economic impacts (see Hallegraeff et al., 2021a). Recent system-specific inter-annual analysis have indeed reported variable HAB trends, depending on species and their functional traits, sites, regions, study periods, and concurrent environmental forcing (Anderson et al., 2021; Belin et al., 2021; Gianella et al., 2021; Hallegraeff et al., 2021a, 2021b; McKenzie et al., 2021; Pitcher and Louw, 2021). Thus, a comprehensive understanding of HAB spatial-temporal variability patterns, bloom phenology, and underlying environmental determinants at the regional level (Gianella et al., 2021; Hallegraeff et al., 2021a), integrated into predictive models, is fundamental for forecasting, mitigating, and effectively managing HABs in coastal waters (see reviews by Franks, 2018, Ralston and Moore, 2020).

Planktonic HABs, like all phytoplankton blooms, result from transient increases of algal abundance, during periods when instantaneous growth overcome mortality rates. Thus, both bottom-up controls, acting directly on phytoplankton growth rates (e.g., light, inorganic nutrients, turbulence), and top-down controls, acting directly on phytoplankton loss rates (e.g., grazing, advection), are potentially relevant environmental drivers of phytoplankton blooms (see review by Barbosa and Chícharo, 2011). In coastal systems, bottom-up and top-down controls of HABs are shaped by multiple forces, including localized anthropogenic, climatologic, hydrographic, and oceanographic processes, and large-scale climatic forces (Anderson et al., 2012; Wells et al., 2015, 2020; Glibert, 2020; Trainer et al., 2020a). Additionally, differences in functional traits between phytoplankton groups, sometimes associated with contrasting niche preferences (see Weithoff and Beisner, 2019), generate variable responses to environmental changes, for different HAB groups (Barton et al., 2013; Glibert and Burford, 2017; Otero et al., 2018; Glibert, 2020). Due to the complexity of HAB patterns and drivers, and consequential limited availability of integrative fully mechanistic-numerical models (e.g., coupled physical-biological model, *Alexandrium catenella,* McGillicuddy et al., 2011 and references therein), empirical-statistical modelling strategies have been frequently used for HAB prediction (see reviews by Rossini, 2014; Franks, 2018; Ralston and Moore, 2020; Cruz et al., 2021), in isolation or combined into hybrid models (e.g., Stumpf et al., 2009; Anderson et al., 2011, 2016; Brown et al., 2013; Davidson et al., 2021; Fernandes-Salvador et al., 2021).

Coastal waters off southern Portugal, and associated coastal lagoons and estuarine systems, are relevant areas for the production and harvesting of wild and farmed shellfish and finfish species, thus are highly susceptible to the detrimental effects of planktonic toxigenic HABs (Vale et al., 2008; Botelho et al., 2019; Bresnan et al., 2021; Cravo et al., 2022). Studies of phytoplankton off southern Portugal have assessed chlorophyll-a variability, phenology (e.g., Cristina et al., 2016; Krug et al., 2017, 2018b; Ferreira et al., 2019, 2021; Santos et al., 2020), and species composition and size structure (e.g., Moita, 2001; Loureiro et al., 2011; Goela et al., 2014; Sañé et al., 2019; Santos et al., 2021). Nonetheless, most comprehensive studies specifically addressing dynamics and drivers of HABs have been focused on the central and northwest Portuguese coasts. Over these regions and, also considering information available for adjacent Spanish (northwest) coastal waters, blooms of *Pseudo-nitzschia* H. Peragallo, 1900, related with the amnesic shellfish poisoning (ASP) syndrome in humans, are recurrent events during the spring-summer upwelling period (Palma et al., 2010; Vidal et al., 2017; Palenzuela et al., 2019). Blooms of Dinophysis Ehrenberg, 1839, associated with diarrhetic shellfish poisoning (DSP) syndrome, are also recurrent off northwestern Iberia during the upwelling season, but favored in periods of thermohaline stratification (Reguera et al., 1995; Moita et al., 2006a, 2016; Escalera et al., 2010; Velo-Suárez et al., 2014; Díaz et al., 2016, 2019; Vidal et al., 2017; Aláez et al., 2021). Blooms of *Gymnodinium catenatum* H.W. Graham, 1943, causative of the paralytic shellfish poisoning (PSP) syndrome, are less recurrent, and more frequent in this domain during autumn, under downwelling conditions (Moita et al., 1998; Sordo et al., 2001; Bravo et al., 2010; Moita et al., 2003; Díaz et al., 2019). Available information on HABs enabled the development of group-specific predictive models for northwestern Iberia (Palma et al., 2010; Moita et al., 2016; Díaz et al., 2016; Ruiz-Villarreal et al., 2016; Palenzuela et al., 2019; Alaéz et al., 2021). By contrast, knowledge of planktonic HABs over the south and southwest Portuguese coasts is still limited (Moita, 2001), mostly covering the westernmost sector of the south coast (Loureiro et al., 2005, 2011; Danchenko et al., 2019; Santos et al., 2021), or specific HAB events (Mateus et al., 2013; Pinto et al., 2016; Caballero et al., 2020). Beyond a mechanistic Lagrangian model previously used for predicting HABs along the southwest and south Portuguese coasts, during a limited period (Silva et al., 2016), no group-specific predictive models for HABs are currently available for the complex coastal domains off southern Portugal.

In this context, the main goal of the current study was to evaluate the spatial-temporal variability patterns and phenology of potentially toxigenic phytoplankton taxa in coastal waters off southern Portugal, during a 6-year period (2014−2019). The specific objectives of this study included: (i) the analysis of intra-annual variability patterns, phenology, and associated environmental drivers for the most frequently reported potentially toxigenic phytoplankton taxa, for different domains of this heterogeneous coastal area, and (ii) the establishment of region-specific empirical statistical models linking the abundance of key potentially toxigenic taxa with influential environmental predictors. Environmental determinants included sea surface temperature, radiation, mixed layer depth, upwelling intensity, riverine freshwater discharge, and chlorophyll-a concentration. Potentially toxigenic phytoplankton taxa comprised two major HAB-forming groups (diatoms and dinoflagellates), with contrasting functional traits and environmental requirements. Based on previous studies (Pitcher et al., 2010; Barton et al., 2013; Behrenfeld et al., 2013; Díaz et al., 2016, 2019; Glibert and Burford, 2017), we hypothesized that diatom blooms will be triggered under turbulent, nutrient-rich upwelling conditions, while dinoflagellate blooms are more likely to be associated with downwelling periods and/or relatively stratified conditions. Additionally, higher prevalence of diatom blooms and lower prevalence of dinoflagellate blooms are expected for study regions under stronger upwelling intensity.

## 2. Material and methods

### 2.1. Study area

The southern Portuguese coast (36° to 38°N and 12° to 5.8°W; see Fig. 1), is located at the northernmost section of the Iberian Canary Eastern Boundary Upwelling system, and partly included in the Gulf of Cadiz, and comprises zonally (south) and meridionally (southwest) oriented coastal stretches. This complex coastal domain, with a continental shelf ranging from 5 to 35 km width, is influenced by different physical oceanographic regimes (García-Lafuente et al., 2006; Relvas et al., 2007), and subjected to variable nutrient-rich freshwater inputs from rivers, including Guadiana, Tinto, Odiel, Guadalquivir (see Fig. 1; e.g., Caballero et al., 2014; Krug et al., 2017), and submarine groundwater discharges (Hugman et al., 2015; Piló et al., 2018). Mesoscale and sub-mesoscale features (e.g., upwelling filaments, fronts, shelf and oceanic cyclonic and anticyclonic eddies, coastal countercurrents), often associated with coastal topography and coastline irregularities including capes (e.g., Cape São Vicente, CSV; Cape Santa Maria, CSM), and canyons, are relevant attributes of the study area (Peliz et al., 2004, 2007, 2009; García-Lafuente et al., 2006; García-Lafuente and Ruiz, 2007;

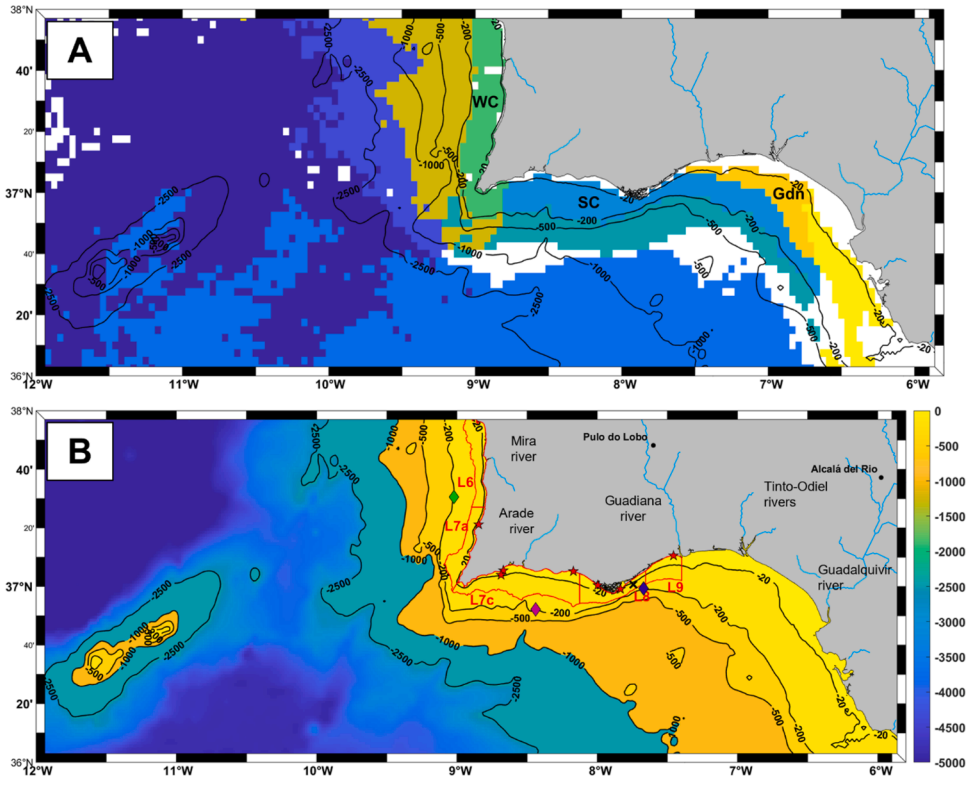


**Fig. 1.** (A) Study area, off southern Portugal, with identification of regions (different colors) with coherent covarying chlorophyll-a variability patterns, as defined by Krug *et al.* (2017), including the coastal regions considered in this study: West Coast (WC), South Coast (SC), and Guadiana (Gdn). (B) Study area, off southern Portugal, with information on bathymetry and major river systems. PL and AR depict the location of Pulo do Lobo and Alcalá del Río hydrographic stations, respectively. Diamonds show the approximate positions of the three sites used for the calculation of the wind-based upwelling index, along the southwest coast (green), and south coast, at western (pink) and eastern (blue) sectors of Cape Santa Maria. Black cross represents the Armona site, where alongshore current velocities were measured. Red stars represent approximate positions of the sampling stations used for the analysis of toxigenic phytoplankton (from north to south and west to east: Aljezur, Porto de Mós, Praia Dona Ana, Falésia, Praia de Faro, Culatra, and Monte Gordo; see text for further details), by the Portuguese Institute of the Sea and Atmosphere (IPMA). Sampling stations are integrated into shellfish coastal production areas (L7a, L7c, L8 and L9), delimited by red polygons. L6 area is limited to the spatial domain considered in this study. Limits of the shellfish coastal production areas retrieved from IPMA (https://www.ipma.pt/en/bivalves/docs/).

Relvas et al., 2007).

This region is subjected to seasonal coastal upwelling, usually intensified during the early spring to late summer period (Fiúza et al., 1982; García-Lafuente and Ruiz, 2007; Relvas et al., 2007, 2009; Arístegui et al., 2009). Along the meridional (southwest) coast, summer northerly winds force offshore transport of near-surface waters, promoting upwelling-favourable conditions. During autumn, this regime is shifted to southerly winds, favouring downwelling conditions (Fiúza et al., 1982; Relvas and Barton, 2002). Along the zonal (south) coast, upwelling conditions are associated with strong westerly winds, but upwelling intensity is lower, diminishing eastward of CSM. During upwelling relaxation, a nearshore, warm coastal countercurrent flows westward, occasionally turning clockwise around CSV, promoting the connectivity between sectors east and west of CSM (Relvas and Barton, 2002; García-Lafuente et al., 2006; Garel et al., 2016). This coastal countercurrent is driven by an alongshore pressure gradient, intensified by wind forcing, and occurs all-year around (ca. 40%), without seasonal variability (Garel et al., 2016; De Oliveira Júnior et al., 2021). Surface circulation in the south Portuguese outer shelf and upper slope domain is affected by the Gulf of Cadiz Current, flowing eastward from CSV to the Strait of Gibraltar. This strong persistent current, intensified east of CSM, may promote the extension of the upwelling current from the southwest coast over the south shelf/slope waters (García-Lafuente et al., 2006; Peliz et al., 2007, 2009). Overall, upwelling patterns have been reported as relevant drivers of phytoplankton variability in the study area (see Krug et al., 2017, 2018b; Ferreira et al., 2021).

### 2.2. Environmental setting

A set of environmental determinants were acquired for the study period (2014–2019) from different sources: satellite remote sensing (wind speed and direction; Sea Surface Temperature, SST; and Photosynthetically Available Radiation, PAR), model-based data (Mixed Layer Depth, MLD), and *in situ* observations (Guadiana and Guadalquivir riverine discharges), at different spatial-temporal resolutions. Due to the absence of site-specific data, collected concurrently with HAB sampling, environmental data were averaged over three different coastal regions, that comprise HAB sampling stations (West Coast, WC; South Coast, SC; and Guadiana, Gdn; see Fig. 1A), identified by a previous objective partition of the study area (Krug et al., 2017). This partition was based on chlorophyll-a variability patterns, used as a proxy for phytoplankton biomass. The partition of the study area based on abiotic variables was not considered due to the reduced number of coastal environmental provinces identified (two; Krug et al., 2018a), that does not reflect phytoplankton dynamics over the area (Krug et al., 2017, 2018b). The use of this chlorophyll-a based partition implicitly assumes that abiotic variables and phytoplankton share similar spatio-temporal variability patterns. Yet, this assumption minimizes the potential role of phytoplankton top-down controls.

#### 2.2.1. Physical oceanographic variables

Level 3, 8-day composites of satellite-derived SST data were retrieved from MODerate resolution Imaging Spectroradiometer, onboard the Aqua satellite (MODISA), available at NASA's Oceancolor database (http://oceancolor.gsfc.nasa.gov/). SST data, at 4 km resolution, was limited to night-time passes, to avoid diurnal solar heating effects (Robinson, 2010), and high-quality data (AVHRR quality flags 6 and 7, and MODIS-A quality flag 0).

Daily MLD data, at ~ 0.083° spatial resolution, was acquired from the Iberian Biscay Irish regional seas (IBI) reanalysis database (Product ID: IBI_REANALYSIS_PHYS_005_002), for the period 2014–2018, provided by Copernicus Marine Service (CMS). This model-derived variable is estimated as the ocean depth at which the water potential density has increased by 0.01 kg $m^{-3}$ relative to the near-surface value at 10 m depth level (CMS; https://marine.copernicus.eu/). Maximum MLD values were limited by local bathymetry. Missing MLD data for the year 2019 were estimated after regressing data from the referred source with data retrieved from the following two datasets: the Hybrid Coordinate Ocean Model (HYCOM), based on the 0.03 kg $m^{-3}$ density threshold (ID: expt_91.0, expt_91.1 and expt_91.2), and available for the period 2014-

2019, at Ocean Productivity (http://sites.science.oregonstate.edu/ocean.productivity/); and IBI ANALYSIS (ID: IBI_ANALYSIS_FORECAST_PHYS_005_001), available for the period 2016-2019, at CMS. Since the best-fitting linear regression model was associated with IBI ANALYSIS product (period: 2016-2018; $N$=1089; $R^2$ ranging 0.47 and 0.74, depending on coastal regions, $p < 0.0001$), this was then used for estimating daily MLD during the year 2019.

Level-3, 8-day composites of mean surface PAR, at 1 km spatial resolution, from MODISA, were also retrieved from NASA's Oceancolor database (http://oceancolor.gsfc.nasa.gov/). PAR vertical attenuation coefficient ($K_{PAR}$, $m^{-1}$) was calculated using Eq. (1), following Rochford et al. (2001), and the light attenuation coefficient at 490 nm wavelength ($K_{490}$, $m^{-1}$) was obtained from the Ocean Colour Climate Change Initiative Group, OC-CCI (https://www.oceancolour.org/). Mean PAR intensity in the mixed layer ($I_m$, μmol photons $m^{-2}$ $s^{-1}$) was estimated using Eq. (2), according to Kirk (1986).

$$K_{PAR} = 0.085 + 1.6243K_{490} \quad (1)$$

$$I_m = I_0\frac{(1 - e^{-K_{PAR}\ MLD})}{K_{PAR}\ MLD} \quad (2)$$

Upwelling intensity was estimated using a wind-based index, the cross-shore Ekman transport (CSET), that represents the magnitude of the offshore component of Ekman transport, comparable to the amount of water upwelled from the base of the Ekman layer (Bograd et al., 2009). Daily sea surface zonal (U) and meridional (V) wind fields, at 0.25º spatial resolution, for the period 2014-−2018, were obtained from the Blended Sea Winds dataset (BSW), available at NCEI-NOAA (https://www.ncdc.noaa.gov/data-access/marineocean-data/blendedhttps://www.ncei.noaa.gov/products/blended-sea-winds). BSW are based on a combination of several scatterometers, standardized across platforms, resulting in high quality ocean wind vectors (Zhang et al., 2006). Missing wind data for the year 2019 were estimated using a linear regression applied to data from the referred source and the dataset, acquired by the Advanced Scatterometer (ASCAT), onboard the Meteorological Operational Satellite-B (MetOp-B) at the same resolution, accessible for the period 2016−2019, retrieved from the Global Ocean L3 Wind Product in CMS (period: 2016-2018; $N$=751 or 809, $R^2$ between 0.54 and 0.61, depending on coastal regions, $p < 0.0001$).

CSET was computed for three locations (see Fig. 1B): one site positioned at ~ 20 km off the southwest Portuguese coast ($CSET_{WC}$), and two sites positioned off the south Portuguese coast, at 24 km and 11 km from the coastline, on the western and eastern sectors of CSM, respectively ($CSET_{wCSM}$ and $CSET_{eCSM}$). For each site, CSET was based on the average data of a 0.75º x 0.75º box centred at the target location. Considering the orientations of the south and southwest Portuguese coastlines (see Fig. 1), for the south coast, $CSET_{wCSM}$ and $CSET_{eCSM}$ were estimated from the meridional component of the Ekman transport, induced by the zonal component of wind-stress. Over the southwest coast, $CSET_{WC}$ was based on the zonal component of the Ekman transport, induced by the meridional component of wind-stress (Bakun, 1973; for more details see Alvarez et al., 2011, and Krug et al., 2017). Negative values of the upwelling index indicate offshore Ekman transport and upwelling-favourable conditions, whereas positive values represent onshore Ekman transport and downwelling-favourable conditions. Limitations of this wind-based upwelling index, namely for coastal bays, were reviewed by Largier (2020).

Additionally, alongshore current velocity, measured at high temporal resolution (1-4 hours) by an Acoustic Doppler Current Profiler (ADCP), moored at 23 m depth level, near Armona island (37º 00.648', -7º 44.480'; see Fig. 1B), was also used as proxy for the physical oceanographic regime over the south-eastern Portuguese coast (see Garel et al., 2016). Current velocity data were filtered using a Butterworth filter of 40 h cut-off period for removing high frequency oscillations (e.g., tides; Garel et al., 2016). Considering the reported duration of upwelling events over the study area (ca. 7 days, Palma et al., 2010), a threshold criterion of at least seven consecutive days of negative (positive) current velocity, associated with westward (eastward) current flow, was used to identify downwelling/countercurrent (upwelling) conditions at the south-eastern Portuguese coast. Periods when the criteria were not met were classified under a mixed physical oceanographic regime.

#### 2.2.2. Hydrographic variables

Guadalquivir river discharge, measured at the Alcalá del Río station during the period 2014−2019, at daily resolution, was acquired from the Spanish Regional Water Management Agency (http://www.chguadalquivir.es/saih/). Guadiana river discharge, measured at the hydrometric station Pulo do Lobo, at daily resolution, during the same period, was accessed from the Portuguese Environmental Agency public database (http://snirh.apambiente.pt/).

### 2.3. Phytoplankton data

Remotely retrieved surface chlorophyll-a concentration (Chl-a) and the abundance of potentially toxigenic phytoplankton groups, hereafter referred as HAB-forming taxa, in different shellfish production areas (see Fig. 1B), were obtained for the period 2014-2019.

#### 2.3.1. Chlorophyll-a concentration

Level 3, 8-day composites of satellite-derived surface Chl-a, at 4 km resolution, used as a proxy for total phytoplankton biomass, was retrieved from the European Space Agency (ESA)'s OC-CCI group (https://www.oceancolour.org/). The OC-CCI Chl-a product combines information from several sensors (Sea-viewing Wide Field of View Sensor, MODISA, Medium Resolution Imaging Spectrometer, and Visible Infrared Imaging Radiometer Suite), enabling an increased spatial-temporal resolution data (Sathyendranath et al., 2019). Chl-a data were averaged for three specific coastal regions, identified by a previous objective partition of the study area based on phytoplankton spatial-temporal variability patterns (Krug et al., 2017): WC, SC, and Gdn areas (see Fig. 1A).

#### 2.3.2. Abundance of HAB-forming taxa

Abundance of the most frequently reported planktonic potential HAB-forming groups in the study area (ASP, DSP, and PSP-producers) was obtained from the Portuguese Institute of the Sea and Atmosphere (IPMA) public database (http://www.ipma.pt/pt/index.html/), for different nearshore sampling stations (from north to south, and west to east: Aljezur, Porto de Mós, Praia Dona Ana, Falésia, Praia de Faro, Culatra, and Monte Gordo; see Fig. 1B) incorporated into different shellfish coastal production areas, hereafter coastal production areas (L7a, L7c, L8, and L9). Additionally, HAB abundance data measured at the three sampling stations located in L6 area (Sesimbra: 38º 26.309', -9º 6.496'; Galapos: 38º 28.815', -8º 58.417'; Comporta: 38º 22.800', -8º 48.500'), retrieved from the same source, were used to characterize the northern domain adjacent to the L7a coastal production area. This dataset was collected by IPMA in the framework of the Portuguese National Bivalve Mollusk Monitoring System, following the requirements of European Community, EC (EC, 2004a, 2004b). Sampling stations have been defined to ensure representativeness of the conditions associated with the sites effectively used for shellfish production, within each coastal area, not necessarily the entire coastal area. Sampling frequency was approximately weekly but intensified during periods of historically high abundances of HAB-forming species and/or concentrations of phytotoxins in bivalve mollusks (May – November), or after occurrences above alert or threshold levels (see IPMA, 2013). Thus, sampling was not synchronized for all sampling sites. Water samples were collected by or under supervision of IPMA technicians, generally at shallow accessible locations, and phytoplankton abundance was evaluated using inverted microscopy and the Utermöhl method (see IPMA, 2013). Since *Pseudo-nitzschia* spp. identification is not possible to species

level using light microscopy, in this database, ASP-producers include the sum of the abundances of two groups: *Pseudo-nitzschia delicatissima* group (cells width <3 μm), and *Pseudo-nitzschia seriata* group (cells width >3 μm). Although, *Pseudo-nitzschia* spp. could comprise toxigenic and non-toxigenic species, for consistency, this group will be hereafter designated as ASP-producers. Abundance of DSP-producers includes the sum of *Dinophysis* spp., *Prorocentrum* spp. (except *P. minimum)*, and *Phalacroma* sp., and abundance of PSP-producers includes the sum of *Gymnodinium* spp. (including *G. catenatum*), *Alexandrium* spp., and *Pyrodinium bahamense var. compressum* (source: https://www.ipma.pt/pt/bivalves/fito/index.jsp).

HAB abundance classified as below the limit of detection (LOD) or 'ND' (undetected) in the IPMA public database were considered as zero. Data with other descriptions including 'NDi' (unavailable), 'NR' (unfulfilled), and 'NQ' (unquantified) were not considered. As information on species-specific abundances at the public database is limited to the period January-October 2014, phytoplankton abundances associated with the human syndromes ASP, DSP, and PSP represent the summation of the abundances of all species potentially linked with each syndrome. Homoyesso- and Yessotoxin-producing dinoflagellates were not included due to their limited occurrence in the study area and period (see IPMA public database).

#### 2.3.3. Phytoplankton phenology

Phenological indices for ASP-, DSP-, and PSP-producers, were estimated using *in-situ* abundance data, retrieved from IPMA public database. For each group and coastal production area, bloom events were defined as occurrences when abundance exceeded 5% above the annual local median value, at least during two consecutive weeks (Siegel et al., 2002), a threshold criterion used in phytoplankton (Ferreira et al., 2014; see Krug et al., 2018b and references therein) and HAB (see Bucci et al., 2020; 5−25%) studies. This approach implicitly considered variable bloom thresholds depending on annual cycles, HAB groups, and coastal production areas, an advantage over recent studies of HAB phenology (Guallar et al., 2017; Karasiewicz and Lefebvre, 2022). Considering all bloom events, for each annual cycle, the following phenological indices were estimated for each coastal production area (L6, L7a, L7c, L8, L9) and HAB group: (1) number of bloom events (bloom events year$^{-1}$); (2) duration of bloom events (weeks bloom$^{-1}$); (3) total duration of all bloom events per year (weeks year$^{-1}$); (4) HAB abundance peak value (cells L$^{-1}$); (5) timing of bloom initiation (i.e., first week when HAB abundance surpassed the threshold criterion; expressed in week of the year, WOY); (6) HAB abundance peak timing (WOY); and (7) timing of bloom termination (last week when HAB abundance was above the threshold criterion; WOY). The beginning of the annual cycle was associated with the first week of January (week 1), ending during the last week of December (week 46).

### 2.4. Data analysis

#### 2.4.1. Nonparametric exploratory analysis

Temporal variability patterns of HABs and underlying environmental determinants were investigated for specific HAB groups and coastal production areas. Differences in abundance and phenological indices between HAB groups and coastal production areas were analyzed using the Kruskal-Wallis test, a one-way analysis of variance on ranks, followed by multiple pair-wise comparisons using the Dunn's test (Dunn, 1961). Spearman rank correlation coefficient ($r_s$) was used to evaluate the strength of monotonic relationships between the abundance of HAB groups and different environmental determinants. All statistical tests were considered at a 0.05 significance level.

#### 2.4.2. Generalized additive models

Generalized Additive Models (GAMs) were developed to identify the most significant environmental predictors of key toxigenic phytoplankton taxa for specific coastal production areas. GAMs are empirical-statistical models, that establish relationships between a dependent response variable and multiple predictors (independent variables; Wood, 2017). Since GAMs do not assume a particular type of response function, allowing both non-linear and linear relationships, they are considered a flexible, computing cost-effective modeling approach for assessing the responses of plankton communities (e.g., Irwin and Finkel, 2008; Llope et al., 2009; Otto et al., 2014), specifically HABs (e.g., Matus-Hernández et al., 2019; Ajani et al., 2020; Boivin-Rioux et al., 2021, 2022), to environmental factors. The basic GAM model structure can be defined as follows (Eq. (3)):

$$Y = \propto + \sum_{j=1}^{n} s_j(X_j) + \varepsilon \quad (3)$$

where Y represents the response variable, ∝ is the intercept, $s_j$ are nonparametric smoothing functions specifying the partial additive effects of each predictor ($X_j$), and ε is a random error term assumed to be normally distributed with zero mean and finite constant variance (Wood, 2017).

In this study, the response variables were the abundance of phytoplankton associated with DSP and ASP syndromes, for different individual (L7a, and L9) or aggregated (L7c-L8) coastal production areas. L7c and L8 areas were aggregated due to the existence of similar phytoplankton variability patterns (Krug et al., 2017). Thus, for each HAB group, a total of three GAM models were developed, for each specific coastal production area. GAM analysis was not applied to PSP-producers due to the limited availability of non-zero observations. Predictor variables included atmospheric and oceanographic variables (SST, PAR, MLD, CSET, alongshore current velocity, Guadiana, and Guadalquivir riverine discharges), and Chl-a, representative of each specific coastal production area. Large-scale climate indices were not considered as model predictors due to their relatively longer variability scales (see Krug et al., 2017 and references therein) in comparison with the length of our study period (6 years). Predictor variables available daily (CSET, alongshore current velocity) were averaged over a 5-day period prior to each sampling date (including the sampling day). Predictor variables available at an 8-day resolution (Chl-a, SST, PAR, MLD), compatible with each sampling date, were averaged over the nearest coastal region (WC, SC, Gdn) of each coastal production area (see Fig. 1A, B). Thus, WC region-averaged values were used as predictors for L7a, SC region-averaged for L7c-L8, and Gdn region-averaged values for L9 coastal production area. Since $CSET_{wCSM}$ and $CSET_{eCSM}$ were not statistically different (Kruskal-Wallis test, N=274, p=0.245), and showed similar temporal variability patterns (Fig. 2C), these two variables were averaged ($CSET_{SC}$), and used as an upwelling index for the aggregated L7c-L8 coastal production areas.

Prior to model development, collinearity between covariate variables was evaluated using Spearman rank correlation coefficients ($r_s$), and variables significantly correlated at $|r_s| > 0.70$ were not used as covariates in the same model run (Dormann et al., 2013). This criterion excluded the use of Chl-a and SST, and PAR and MLD in the same model run, for all coastal production areas. GAM models were fitted using a forward stepwise process (see Zuur et al., 2009), and best-performing models were selected using the following criteria: (1) maximize R-square ($R^2$), and deviance values ($R^2$x100); (2) minimize Akaike Information Criterion (AIC) scores; (3) use predictors that exhibit statistically significant ($p$-value<0.05) relationships with the response variables; and (4) use predictors whose confidence envelopes for the smoothing function do not include zero throughout the covariate range (Wood, 2017; Zarauz et al., 2007; Llope et al., 2009).

Following Zuur *et al.* (2009), different distribution families for the dependent variable, and link functions that relate the mean of the response variable with a smoothed function of the explanatory variables (Hastie and Tibshirani, 1990), were tested for achieving the best models. As the analysis of data frequency distribution indicated that HAB abundance data were unimodal and right skewed, for both groups (DSP

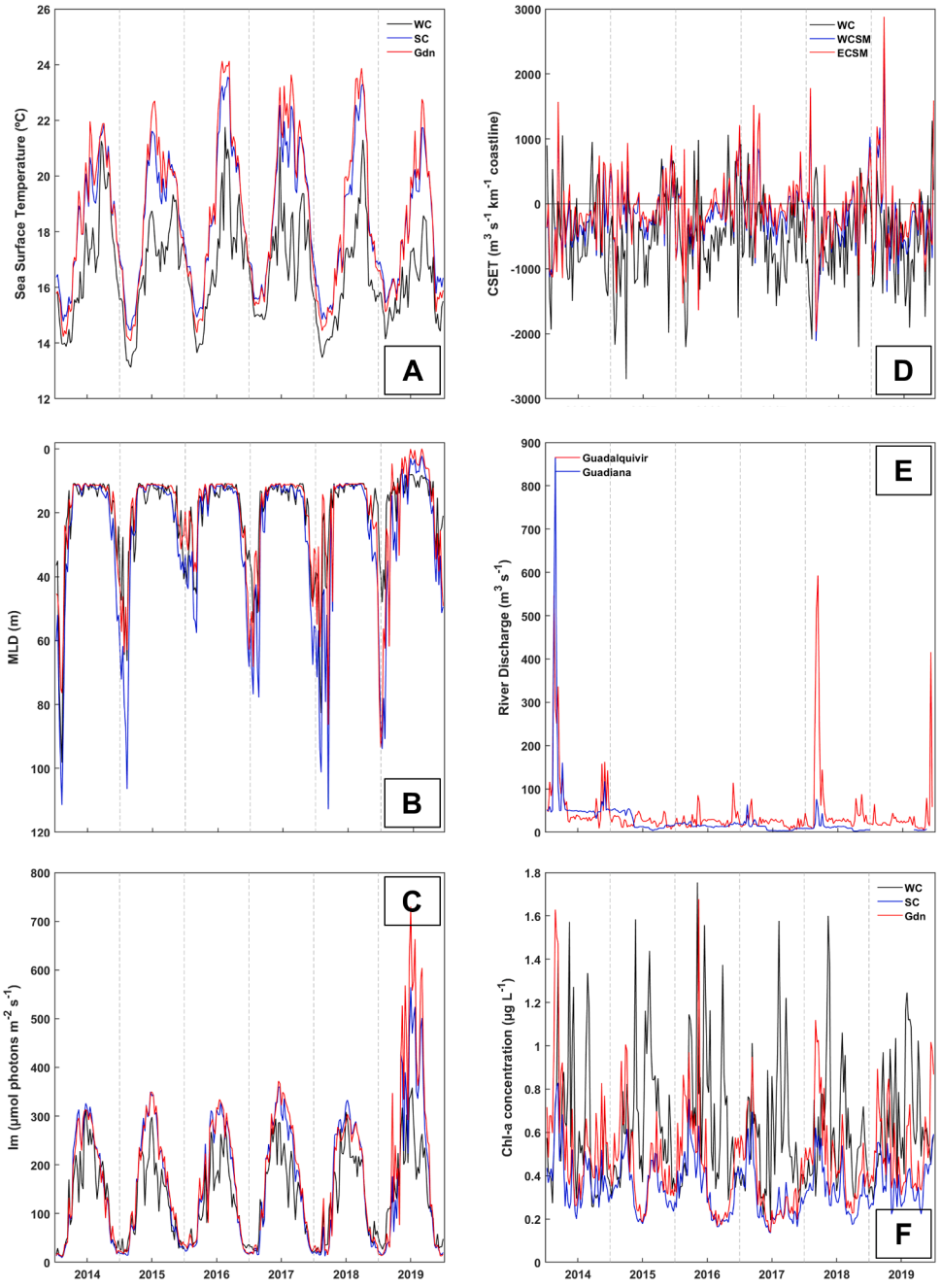


**Fig. 2.** Time series of weekly (8-day) data for selected environmental variables, during the period 2014 - 2019, including: (A) Sea surface temperature (SST), (B) Mixed layer depth (MLD), (C) Mean photosynthetically available radiation in the mixed layer ($I_m$), (D) Cross-shore Ekman transport (CSET) for the south-west coast (WC), and south coast, at western (WCSM) and eastern sectors (ECSM) of Cape Santa Maria, (E) Guadiana and Guadalquivir river discharge, and (F) Chlorophyll-a concentration (Chl-a). SST, MLD, $I_m$, and Chl-a were averaged for three specific coastal regions: West Coast (WC), South Coast (SC), and Guadiana (Gdn). See Fig. 1 for location of specific coastal regions.

and ASP-producers) and all coastal production areas, and normality tests (e.g., quantile-quantile plot, Shapiro-Wilks test) confirmed non-normality, the Gaussian distribution was not considered, and alternative distributions were tested. Firstly, a Poisson distribution with a log link function was used and, after attaining the best model, the amount of overdispersion in the abundance data (i.e., sum of squared Pearson residuals divided by sample size minus the number of parameters) was calculated (Hilbe, 2011; Zuur, 2012). As recommended by Zuur *et al.* (2009), for low overdispersion (above 1.5) a quasi' correction was applied, and for high overdispersion (above 15 or 20), alternative distribution families were tested. Hence, a Negative Binomial (NB) distribution with a log link function was applied. For both DSP and ASP groups, NB with a log link function was the most suitable distribution, since it minimized overdispersion to acceptable levels (0−2.5).

Underlying statistical assumptions (residuals normality, homoscedasticity) of GAMs were tested using visual inspection of graphical residual diagnostics (including quantile-quantile plots, histogram of residuals, and residuals versus predictors plots). Model residuals were tested for temporal autocorrelation, using autocorrelation and partial autocorrelation functions (acf and pacf). As results showed lag-1 partial temporal autocorrelations in all cases, when possible, GAMs were extended to Generalized Additive Mixed Models (GAMMs) by including a first order autoregressive correlation structure, ARMA (e.g., Thackeray et al., 2008; Otto et al., 2014; Krug et al., 2017).

GAMs/GAMMs were also used to decompose HAB temporal variability into intra-annual and interannual components. Response variables were modelled as a cyclic spline smoother function of the month, and a cubic spline smoother function of the year, including a first order autoregressive correlation structure. If GAMM models failed to converge, the corresponding GAM models were selected. Due to the relatively short study period (6-year), the interannual patterns were not further explored. GAM and GAMM analyses were conducted using the

package 'mixed GAM computation vehicle' (mgcv), specifically the 'gam' function, in R statistical software version 4.0.3 (R Core Team, 2020). Other graphical representations were generated using MATLAB 9.8.0.1380330 software (R2020a), with in-house scripts.

## 3. Results

### 3.1. Environmental setting

Basic statistical information on abiotic environmental variables and Chl-a, for different coastal regions off southern Portugal (WC, SC, Gdn), is summarized in Table 1. Considering spatial patterns, higher mean SST values were detected over the south Portuguese coastal regions (SC and Gdn), in respect to WC region ($p<0.05$; see Fig. 2A). MLD values were lower over the Gdn region ($p < 0.05$), but similar for WC and SC regions (Fig. 2B). Both $K_{PAR}$ and $I_m$ mean values were statistically similar for all regions (see Table 1), but $I_m$ generally showed higher values over the south Portuguese coastal regions (SC and Gdn; Fig. 2C). Mean upwelling intensity, estimated for three locations (see Fig. 1) using CSET, was higher over the southwest Portuguese coast, in comparison with the location eastern of CSM ($p < 0.05$). Yet, no difference in upwelling intensity was detected between the eastern and western locations of CSM, along the south Portuguese coast (Fig. 2D). Regarding riverine freshwater fluxes, Guadiana and Guadalquivir average discharge was 29.6 ± 76.5 $m^3\ s^{-1}$, and 43.5 ± 81.1 $m^3\ s^{-1}$, respectively (see Table 1 and Fig. 2E).

With respect to temporal variability, minimum SST values were observed during February-March, while maxima occurred in August-September. Higher summer SST values were generally detected during the year 2016, for all coastal regions, and lower during 2017 and 2019, namely over WC region (Fig. 2A). Deeper MLD, but highly variable between years, were detected during the winter season (January-March), while shallower mixed layers were observed between late-spring and early autumn, for all coastal regions (Fig. 2B). Higher $I_m$ was consistently detected during late-spring or early summer (June-July; Fig. 2C), a period of relatively shallow MLD and elevated PAR (data not shown). According with CSET, upwelling favourable conditions generally prevailed during the spring-summer period (Fig. 2D), for both the southwest and south Portuguese coasts, with longer, stronger events during summer 2015 (south), 2017 (southwest), and 2019 (both). However, strong upwelling-favourable events were detected in all seasons (e.g., winter 2016 and 2018, southwest coast; Fig. 2D). In contrast with CSET data, alongshore current velocity data, measured with a higher frequency at Armona site, showed no clear upwelling/downwelling seasonal patterns for the area east of CSM (see Fig. S1, henceforth S-denote figures and tables refer to supplementary material). Over this area, upwelling (70% occasions) prevailed over downwelling/coastal countercurrent favourable conditions (30%), but the mean duration of upwelling and downwelling events was similar (11.4 ± 4.9 days, and 11.6 ± 3.7 days, respectively; data not shown). Guadiana and Guadalquivir river discharge data showed higher values during the autumn-winter period, with notable late-winter maxima (February-March) during the years 2014 and 2018 (Fig. 2E).

Chl-a, also used as a potential predictor of HABs, showed lower mean values over SC (0.38 ± 0.40 μg $L^{-1}$), intermediate for Gdn, (0.54 ± 0.58 μg $L^{-1}$), and higher values for the WC coastal region (0.61 ± 0.40 μg $L^{-1}$; $p<0.01$; see Table 1 and Fig. 2F). Over WC and SC regions, Chl-a showed a bimodal annual pattern, with late-winter and summer maxima. At SC region, late-winter Chl-a peak surpassed the summer peak, while the opposite occurred for the WC region. The coastal region more influenced by river flow (Gdn) exhibited more variable patterns, ranging from uni- to bimodal annual cycles, with maxima during March for most years (Fig. 2F).

**Table 1**
General statistical information, including mean, standard deviation (SD), minimum (Min) and maximum (Max) values, and number of samples (N), for physical variables (sea surface temperature, SST; intensity of photosynthetically available radiation at the surface, PAR; PAR light attenuation coefficient, $K_{PAR}$; mean PAR intensity in the mixed layer, $I_m$; mixed layer depth, MLD; and cross-shore Ekman transport, CSET), hydrographic variables (Guadiana and Guadalquivir river discharge), and chlorophyll-a concentration (Chl-a) during the period 2014-2019. Values of SST, PAR, $I_m$, $K_{PAR}$, MLD, and Chl-a were integrated over three specific coastal regions off southern Portugal (West Coast, WC; South Coast, SC; and Guadiana, Gdn), PL and AR: Pulo do Lobo and Alcalá del Río hydrometric stations. See Fig. 1 for location of coastal regions.

| Variable | Region | Mean | SD | Min | Max | N |
|---|---|---|---|---|---|---|
| SST (°C) | WC | 16.5 | 1.8 | 13.1 | 21.8 | 276 |
| | SC | 18.4 | 2.3 | 14.5 | 23.6 | 276 |
| | Gdn | 18.5 | 2.7 | 14.1 | 24.1 | 276 |
| PAR (μmol photons $m^{-2}$ $s^{-1}$) | WC | 460.1 | 181.0 | 135.3 | 742.3 | 276 |
| | SC | 469.6 | 185.0 | 143.3 | 744.7 | 276 |
| | Gdn | 469.6 | 186.6 | 137.5 | 746.2 | 276 |
| $K_{PAR}$ ($m^{-1}$) | WC | 0.1 | 0.02 | 0.04 | 0.2 | 276 |
| | SC | 0.1 | 0.02 | 0.04 | 0.1 | 276 |
| | Gdn | 0.1 | 0.03 | 0.04 | 0.2 | 276 |
| $I_m$ (μmol photons $m^{-2}$ $s^{-1}$) | WC | 134.5 | 86.7 | 9.3 | 358.4 | 276 |
| | SC | 164.2 | 128.9 | 9.9 | 564.8 | 276 |
| | Gdn | 177.1 | 140.1 | 12.5 | 730.5 | 276 |
| MLD (m) | WC | 20.3 | 14.4 | 7.6 | 98.2 | 274 |
| | SC | 27.2 | 23.1 | 2.2 | 112.8 | 274 |
| | Gdn | 20.7 | 16.8 | 0.02 | 93.43 | 274 |
| CSET ($m^3$ $s^{-1}$ $km^{-1}$ coastline) | WC | -508.2 | 1032.0 | -7855.3 | 4928.2 | 2 092 |
| | WCSM | -193.0 | 778.5 | -6461.0 | 4601.3 | 2 071 |
| | ECSM | -112.7 | 866.6 | -5292.3 | 10570.0 | 2 068 |
| Along-shore current velocity (m $s^{-1}$) | Armona | 0.1 | 0.1 | -0.2 | 0.3 | 2 829 |
| Guadiana discharge ($m^3$ $s^{-1}$) | PL | 29.6 | 76.5 | 0.9 | 1003.7 | 1 913 |
| Guadalquivir discharge ($m^3$ $s^{-1}$) | AR | 43.5 | 81.1 | 0.3 | 1105.0 | 2 191 |
| Chl-a (μg $L^{-1}$) | WC | 0.63 | 0.30 | 0.19 | 1.75 | 276 |
| | SC | 0.35 | 0.13 | 0.14 | 0.83 | 276 |
| | Gdn | 0.48 | 0.24 | 0.14 | 1.68 | 276 |

### 3.2. Spatial-temporal variability patterns of HAB-forming taxa

Basic statistical information on the abundance of HAB-forming phytoplankton, for different spatial domains off southern Portugal, is summarized in Table 2. Region-specific mean abundance of ASP-producers ranged from 9942.3 ± 22267.1 cells $L^{-1}$ to 25138.9 ± 74882.9 cells $L^{-1}$ at L6 and L7c coastal production areas, respectively, and abundances at L7a, L8 and L9 were lower than at L6 and L7c areas ($p<0.05$; Fig. 3). Mean abundance of DSP-producers varied from 227.5 ± 946.8 cells $L^{-1}$ to 2473.1 ± 40266.2 cells $L^{-1}$ at L8 and L7a areas, correspondingly. Higher DSP abundances were detected at L8 compared to L9 and L7a areas, as well as over L9 with respect to L7a ($p<0.05$; Fig. 3). Mean region-specific abundance of PSP-producers, lower than other HAB-groups ($p<0.01$), fluctuated between 37.2 ± 228.5 cells $L^{-1}$ and 110.7 ± 471.8 cells $L^{-1}$ at L7a and L8, respectively, and higher PSP abundances were detected over L8 and L9 areas ($p< 0.05$), with lowest abundances at L7a area (Fig. 3). Overall, L7a coastal production area generally showed lower abundances for all HAB groups considered.

In general, ASP-producers followed a bimodal annual cycle, with peak abundances occurring during spring (March-April) and summer (July-August, L6, L7c, L8) or autumn (November, L9; Fig. 4, left column). L7a showed a quasi-unimodal cycle, with maxima in July. During the study period, abundances of ASP-producers were mostly lower than the IPMA regulatory alert level (80.000 cells $L^{-1}$), surpassing occasionally this level only at L6/L7a (2% samples) and L7c (8% samples) coastal production areas (Fig. 5). GAM analyses also revealed highly

**Table 2**
General statistical information, including mean, standard deviation (SD), minimum (Min) and maximum (Max) values, and number of samples (N), for the abundance of three toxigenic phytoplankton groups responsible for ASP (Amnesic Shellfish Poisoning), DSP (Diarrhetic Shellfish Poisoning) and PSP (Paralytic Shellfish Poisoning) human syndromes, for different shellfish coastal production areas off southern Portugal (L6, L7a, L7c, L8 and L9), during the period 2014-2019. bd: below detection level. See Fig. 1 for location of shellfish coastal areas. N corresponds to the number of exact available measurements for each coastal production area.

| Variable | Production Area | Mean | SD | Min | Max | N |
|---|---|---|---|---|---|---|
| ASP-producing species (x $10^3$ cells $L^{-1}$) | L6 | 9.9 | 22.3 | bd | 226.0 | 347 |
| | L7a | 13.3 | 55.1 | bd | 812.0 | 290 |
| | L7c | 25.1 | 74.9 | bd | 732.1 | 435 |
| | L8 | 11.2 | 37.8 | bd | 311.5 | 345 |
| | L9 | 13.2 | 41.8 | bd | 433.1 | 299 |
| DSP-producing species (x $10^3$ cells $L^{-1}$) | L6 | 0.7 | 10.4 | bd | 192.9 | 347 |
| | L7a | 2.5 | 40.3 | bd | 685.7 | 290 |
| | L7c | 1.2 | 20.6 | bd | 429.2 | 435 |
| | L8 | 0.2 | 0.9 | bd | 13.8 | 345 |
| | L9 | 0.4 | 4.2 | bd | 72.1 | 299 |
| PSP-producing species (cells $L^{-1}$) | L6 | 43.7 | 297.7 | bd | 4750.0 | 347 |
| | L7a | 37.2 | 228.5 | bd | 3200.0 | 290 |
| | L7c | 43.7 | 249.4 | bd | 3560.0 | 435 |
| | L8 | 110.7 | 471.8 | bd | 4840.0 | 345 |
| | L9 | 83.0 | 347.4 | bd | 3040.0 | 299 |

significant ($p<0.001$) unimodal (L7a) and bimodal (L6/L7c-L8 areas) intra-annual variability patterns for ASP-producers, for all production areas except L9. Less significant interannual non-linear increasing trends at L6 ($p<0.01$), and L7c-L8 areas ($p<0.05$) were also detected (see Fig. S2). Several intense ASP bloom events were detected for adjacent coastal production areas along the south coast, almost synchronously (spring 2014, at L7c and L8; spring and summer 2015, at L7c, L8 and L9), whereas some intense events were detected only at non-adjacent areas (summer 2016, at L7a and L9) or only at one coastal production area (e.g., summer 2018, L6; see Fig. 5). During years of highest (summer) upwelling intensity at the southwest coast (2017 and 2019), the relative similarity in intra-annual variability of ASP-producers pointed to an increased connectivity between L6, L7a and L7c coastal areas (see Fig. 5).

DSP-producers exhibited a unimodal annual cycle, with maxima during spring (April and June, at L8 and L6 areas, respectively) or summer (July-September, for other areas; Fig. 4, middle-column). During the study period, IPMA regulatory alert level for DSP-producers (200 cells $L^{-1}$) was surpassed, every year, in all coastal production areas (L6: 9% samples; L7c: 14%; L8: 17%; and L9: 8%) except L7a (only 2015−2016, and 2018-2019, 4% samples; Fig. 6). GAM analyses also revealed highly significant ($p<0.001$) unimodal intra-annual variability patterns for DSP-producers, and non-linear interannual increasing trends for all coastal production areas, less significant only for the L7c-L8 area ($p<0.01$; see Fig. S3). Several intense DSP bloom events were detected for multiple adjacent coastal production areas, almost synchronously (e.g., summer 2014, at L7c, L8 and L9; spring 2016, at L7c and L8; spring 2018, at most areas; Fig. 6).

The abundance of PSP-producers (see Fig. 4, right column, and Fig. 7) at L6 and L7a areas showed two periods of high variability, with maxima during late-winter – spring (March-May), and summer (July-August). For other areas, maxima were generally detected during early-spring (L8, L9) and mid-spring to summer (L7c), with occasional events during late-winter. For this group, the abundance exceeded IPMA threshold alert level (500 cells $L^{-1}$) only for 1% and 5% of samples, at L6 and L8 areas, respectively (Fig. 7). GAM analyses revealed significant unimodal (L7c-L8, L9 areas; $p<0.01$) and bimodal (L7a; $p<0.001$) intra-annual variability patterns for PSP-producers, and variable interannual trends across coastal production areas (see Fig. S4).

### 3.3. Phenology of HAB-forming taxa

Basic statistical information on phenological indices for different HAB-groups and coastal production areas is summarized in Table S1. Blooms of DSP-, ASP- and PSP-producers represented 43%, 41% and 16%, respectively, of all bloom events detected (total: 128 events). Overall, the frequency and duration of ASP and DSP bloom events were higher than PSP blooms ($p<0.05$; Fig. 8A−D), and peak abundances were lower for PSP blooms, intermediate for DSP blooms ($p<0.05$), and higher for ASP blooms ($p<0.01$; Fig. 8K, L). Bloom initiation and peak timings of DSP-blooms were delayed with respect to winter-spring ASP-blooms ($p<0.01$), and PSP-blooms ($p<0.05$), and anticipated with respect to the summer-autumn ASP-blooms ($p<0.01$). Differences in

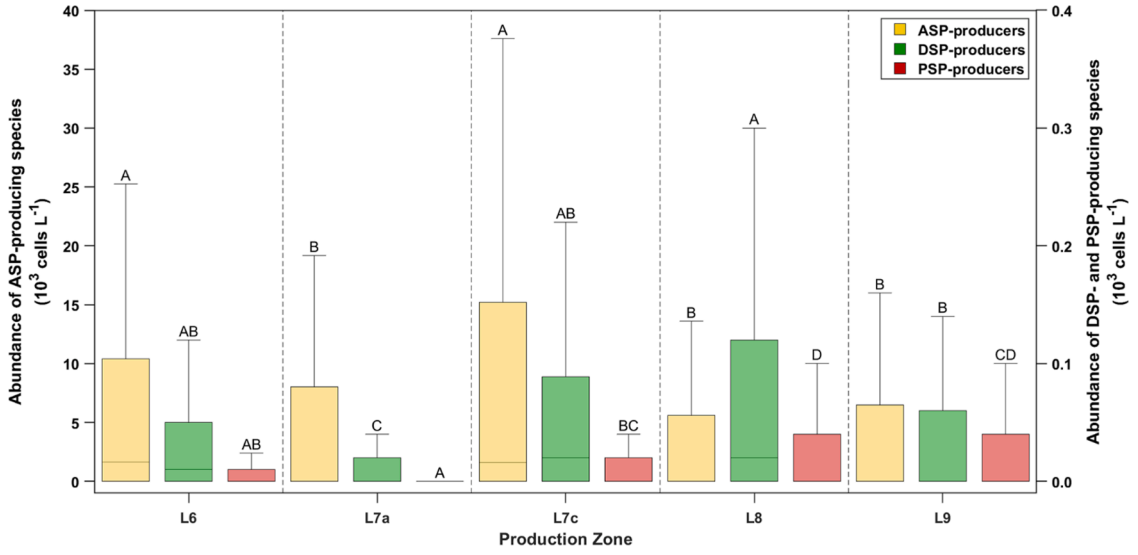


**Fig. 3.** Distribution of the abundance of ASP (Amnesic Shellfish Poisoning), DSP (Diarrhetic Shellfish Poisoning) and PSP (Paralytic Shellfish Poisoning)-producing species, represented by yellow, green, and red colors, respectively, in different shellfish coastal production areas off southern Portugal (L6, L7a, L7c, L8, L9), during the period 2014-2019. Note differences in scale between harmful algal bloom (HAB) groups. Median values are identified by the central line within the box, the bottom and top edges of the box indicate the 25th and 75th percentiles, respectively, and the whiskers represent non-outlier limits. For each group, different uppercase letters over the bars denote significant differences across regions ($p<0.05$). See Fig. 1 for location of sampling sites and shellfish coastal production areas.

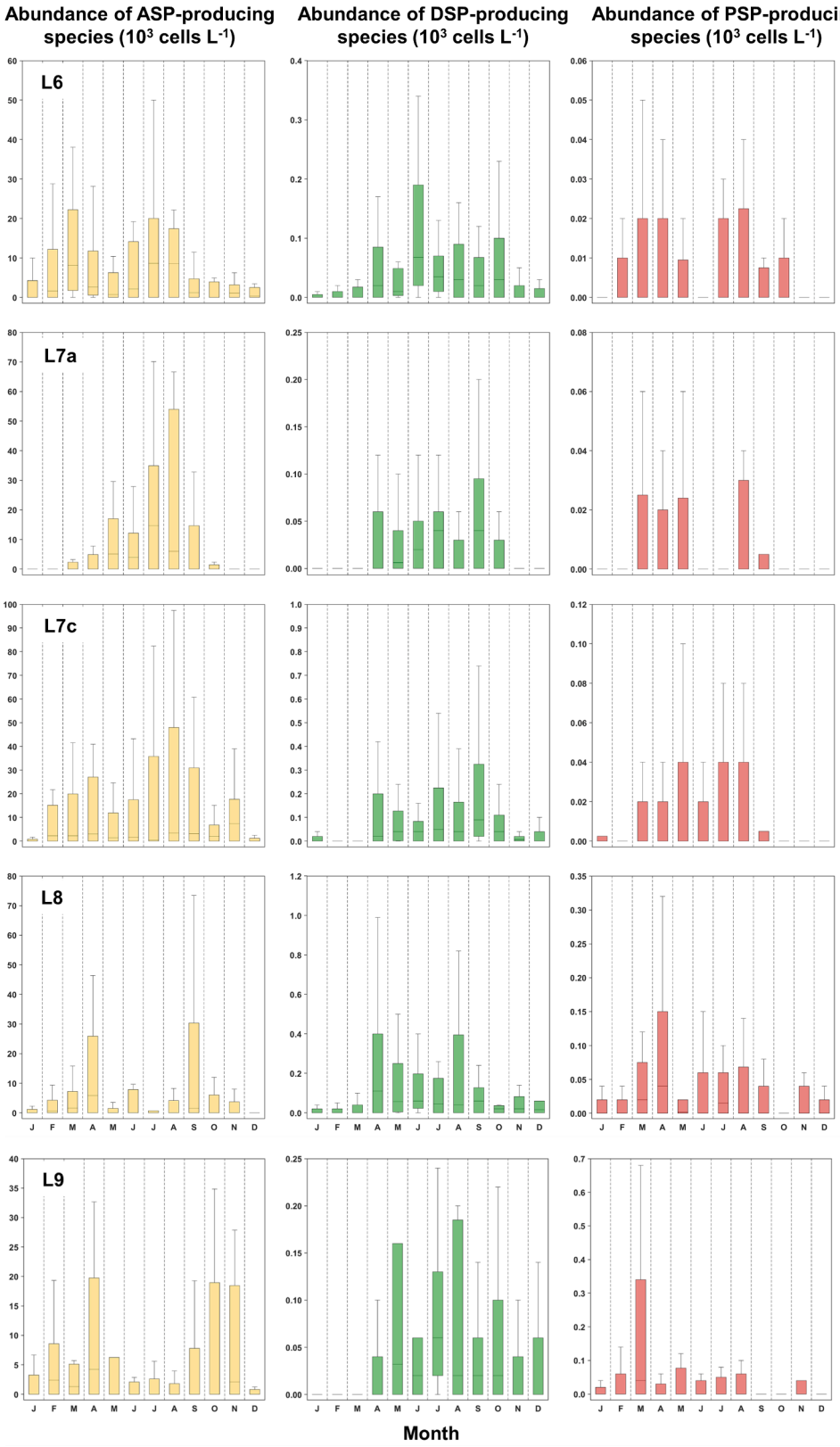


**Fig. 4.** Monthly distribution of the abundance of ASP (Amnesic Shellfish Poisoning), DSP (Diarrhetic Shellfish Poisoning) and PSP (Paralytic Shellfish Poisoning)-producing species, represented by yellow, green, and red colors, respectively, for different shellfish coastal production areas off southern Portugal (L6, L7a, L7c, L8, L9), during the period 2014-2019. Median values are identified by the central line within the box, the bottom and top edges of the box indicate the 25th and 75th percentiles, respectively, and the whiskers represent non-outlier limits. Note differences in scale between harmful algal bloom (HAB) groups. See Fig. 1 for location of sampling sites and shellfish coastal production areas.

phenological indices across coastal production areas were observed only for ASP-producers.

For ASP-producers, the median number of bloom events per year ranged from 1.0 bloom $yr^{-1}$ (L7c, L8) to 3.0 blooms $yr^{-1}$ (L6), with higher bloom frequency for the later (southwestern) coastal production area ($p<0.05$; Fig. 8B). Median bloom duration (Fig. 8D), similar across areas, varied between 3.0 weeks $bloom^{-1}$ (L7a, L7c, L8, L9) and 4.0 weeks $bloom^{-1}$ (L6). Total duration of bloom events per year caused by ASP-producers ranged, considering the median value, from 4.0 weeks $yr^{-1}$ (L7c, L8) to 11.0 weeks $yr^{-1}$ (L6), with a longer duration for L6 with

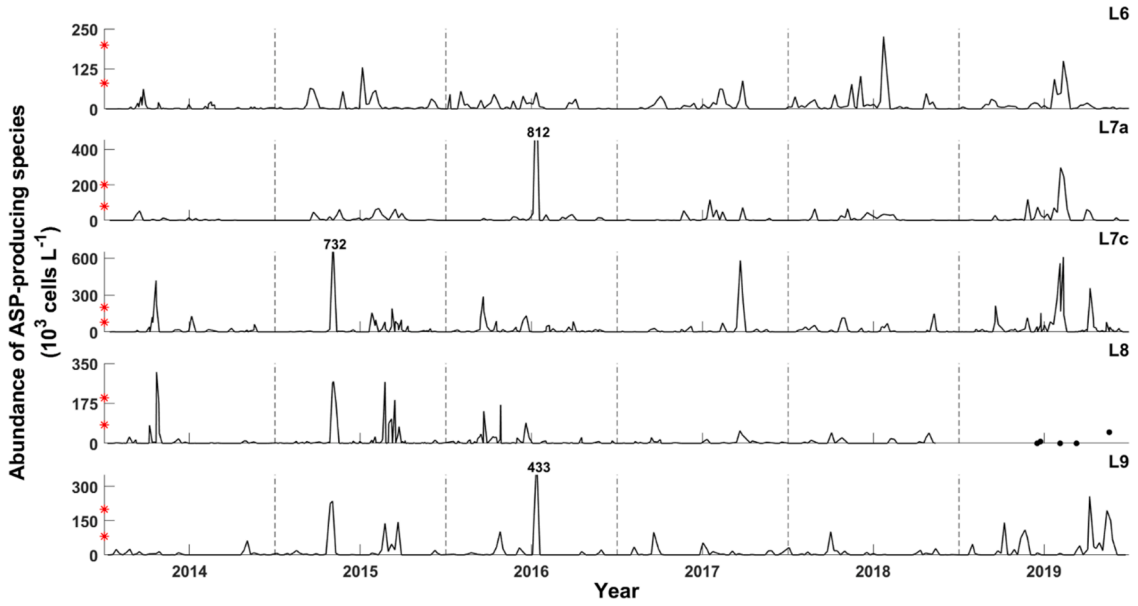


**Fig. 5.** Time series of weekly abundance of Amnesic Shellfish Poisoning (ASP)-producing species, for different shellfish coastal production areas off southern Portugal (L6, L7a, L7c, L8, L9), during the period 2014-2019. Numbers associated with peak values correspond to extreme, out-of-scale observations. Red asterisks on the y-axis indicate the minimum regulatory alert level ($80\times10^3$ cells $L^{-1}$) and interdiction level ($200\times10^3$ cells $L^{-1}$) for this harmful algal bloom (HAB) group. See Fig. 1 for location of sampling sites and shellfish coastal production areas.

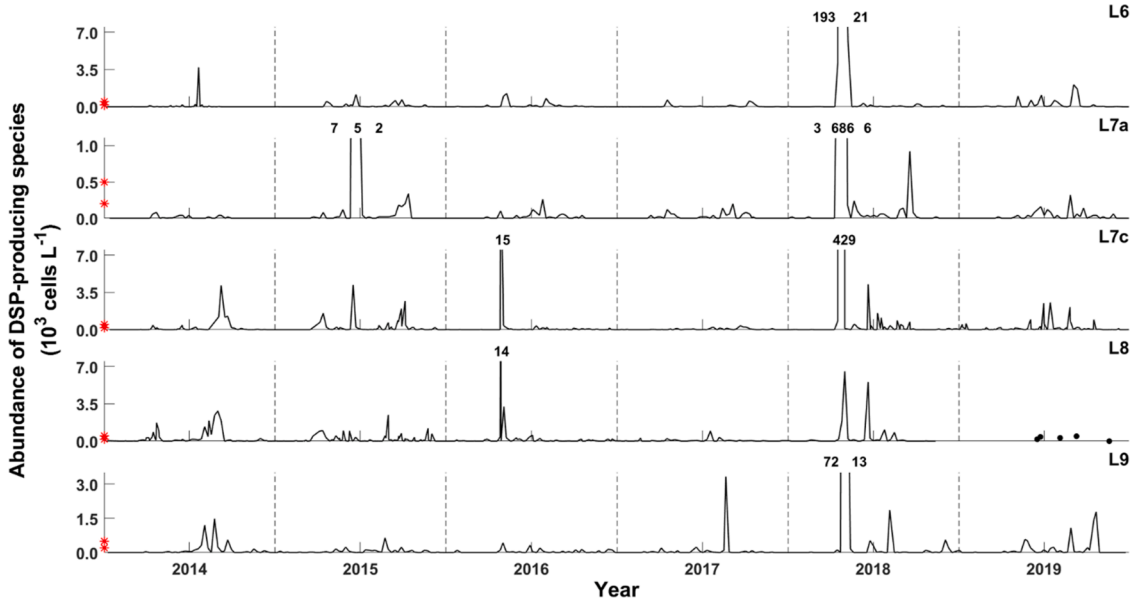


**Fig. 6.** Time series of weekly abundance of Diarrhetic Shellfish Poisoning (DSP)-producing species, for different shellfish coastal production areas off southern Portugal (L6, L7a, L7c, L8, L9), during the period 2014-2019. Numbers associated with peak values correspond to extreme, out-of-scale observations. Red asterisks indicate the minimum regulatory alert level ($0.2\times10^3$ cells $L^{-1}$) and interdiction level ($0.5\times10^3$ cells $L^{-1}$) for this harmful algal bloom (HAB) group (200 cells $L^{-1}$). See Fig. 1 for location of sampling sites and shellfish coastal production areas.

respect to L8 area ($p<0.05$), generally reflecting the variability in bloom frequency across areas (Fig. 8F). Considering that ASP-producers generally showed a bimodal annual cycle, bloom timings and peak values were evaluated for the winter-spring (January-June) and summer-autumn (July-December) periods, separately. Bloom timings for ASP blooms during winter-spring and summer-autumn were different for all coastal production areas ($p<0.05$), but for each bloom period, no differences in bloom timings were detected across coastal areas (Fig. 8H, J). Median bloom initiation timing for winter-spring ASP blooms occurred between March and May (WOY: 9–16; Fig. 8H), peak abundances ($4.0\times10^4$ – $1.0\times10^5$ cells $L^{-1}$; Fig. 8L) were attained in the same period (WOY: 11-17; Fig. 8J), and bloom termination occurred between April and July (WOY: 13–23; see Table S1). For later, summer-autumn ASP blooms, median bloom initiation timing occurred between July and September (WOY: 24–34; Fig. 8H), peak abundances ($3.1\times10^4$ – $1.1\times10^5$ cells $L^{-1}$; Fig. 8L) were achieved from August until October (WOY: 28–35; Fig. 8J), and bloom termination occurred between August and November (WOY: 30–41; see Table S1).

For DSP-producers, median values for bloom frequency, bloom duration, and total duration of bloom events per year were 2.0 blooms $yr^{-1}$, 3.4 weeks $bloom^{-1}$, and 6.4 weeks $yr^{-1}$, respectively, with no differences across coastal production areas (Fig. 8A, 8C, and 8E). Median

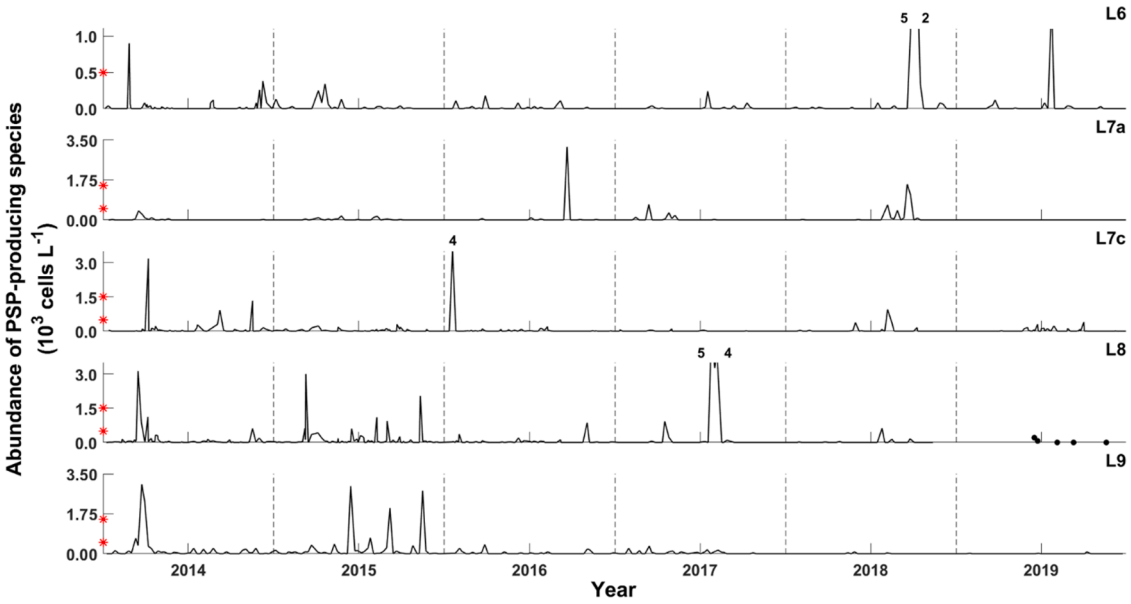


**Fig. 7.** Time series of weekly abundance of Paralytic Shellfish Poisoning (PSP)-producing species, for different shellfish coastal production areas off southern Portugal (L6, L7a, L7c, L8, L9), during the period 2014-2019. Numbers associated with peak values correspond to extreme, out-of-scale observations. Red asterisks represent the regulatory minimum alert level ($0.5\times10^3$ cells $L^{-1}$) and interdiction level ($1.5\times10^3$ cells $L^{-1}$). See Fig. 1 for location of sampling sites and shellfish coastal production areas.

bloom initiation timing was detected in early-June (WOY: 20; Fig. 8G), peak abundances (520 cells $L^{-1}$; Fig. 8K) in late-June (WOY: 22; Fig. 8I), and bloom termination in late-July (WOY: 27; see Table S1). For PSP-producers, median values for bloom frequency, bloom duration, and total duration of bloom events per year were 0.5 blooms $yr^{-1}$, 1.1 weeks $bloom^{-1}$, and 1.1 weeks $yr^{-1}$, respectively, with no differences across coastal production areas (Fig. 8A, 8C, and 8E). Median bloom initiation was observed in mid-March (WOY: 11; Fig. 8G), peak abundances (100 cells $L^{-1}$; Fig. 8K) in early-April (WOY: 13; Fig. 8I), and bloom termination in May (WOY: 16; see Table S1).

### 3.4. *Environmental predictors of harmful algal blooms*

A summary of the best-performing GAM models applied to ASP- and DSP-producers, for different coastal production areas is provided in Table 3. For ASP-producers, the best-performing GAM models showed relatively reduced explanatory power (7-8%), and significant predictors varied across coastal areas (Fig. 9 and Table S2). At L7a area, PAR, the only significant predictor ($p<0.001$), presented a positive linear effect, with positive anomalies for PAR values above ca. 500 μmol photons $m^{-2}$ $s^{-1}$. For L7c-L8 areas, MLD and SST were the most significant predictors ($p<0.001$), both showing non-linear negative effects, and positive anomalies in ASP abundance were associated with MLD values below ca. 20 m, and SST below ca. 20 ºC. Guadalquivir river discharge was also identified as a predictor for L7c-L8 areas ($p<0.01$), with *quasi* linear negative effects. At L9 area, alongshore current velocity and Guadiana river discharge were the most relevant predictors of ASP-producers, but the significance level was generally low ($p<0.05$). Alongshore current velocity exerted a positive linear influence on the abundance of ASP-producers, while Guadiana river discharge presented a negative *quasi* linear effect. Positive anomalies in ASP abundance were associated with positive along-shore current velocity, representative of upwelling-favourable conditions over this area, and river discharge below ca. 20 $m^3$ $s^{-1}$ (Fig. 9).

For DSP-producers, the best-performing GAM models showed higher explanatory power (21−54%), and the relevant predictors also differed across coastal production areas (Fig. 10 and Table S3). The percentage of variance explained by DSP-models decreased from the southwest Portuguese coast (L7a; 54%), westward along the south coast (L7c-L8, L9; 21−36%). At L7a area, the most significant predictor of DSP-producers was Chl-a ($p<0.001$), with non-linear positive effects for Chl-a values from ca. 0.3 to 0.6 μg $L^{-1}$, and negative effects for higher Chl-a values. MLD showed non-linear negative effects on DSP abundance ($p<0.001$), for MLD values below ca. 50 m. Partial effects of PAR were non-linear ($p<0.001$), with a negative influence for PAR between 300 and 400 μmol photons $m^{-2}$ $s^{-1}$, and a positive influence for higher values. SST, the least significant predictor for L7a area ($p<0.01$), generally showed partial negative effects for values up to 18 ºC (Fig. 10). Along the south Portuguese coast, and for L7c-L8 areas, PAR was the most relevant predictor of DSP-producers ($p<0.001$), with positive non-linear effects for PAR up to ca. 600 μmol photons $m^{-2}$ $s^{-1}$ (Fig. 10). Chl-a showed a positive influence up to ca. 0.3 μg $L^{-1}$, and a negative influence for higher values ($p<0.001$). As referred for ASP-producers, Guadalquivir river discharge was also a significant predictor of DSP-producers for this coastal area ($p<0.01$), showing a modest positive influence for discharge below ca. 200 $m^3$ $s^{-1}$, and a negative influence for higher river discharge. Negative anomalies in DSP abundance were associated with positive alongshore current velocity, indicative of upwelling-favourable conditions (Fig. 10). Over L9 coastal area, PAR was the most influential predictor ($p<0.001$), as for L7c-L8 area, showing linear positive effects, and positive anomalies in DSP abundance for PAR values above ca. 500 μmol photons $m^{-2}$ $s^{-1}$. Guadiana river discharge and alongshore current velocity were also relevant, but less significant predictors ($p<0.05$). Guadiana discharge presented linear negative effects on the abundance of DSP-producers, and alongshore current velocity exhibited non-linear positive effects, intensified during upwelling conditions (Fig. 10).

The limited availability of non-zero abundances of PSP-producers precluded the application of GAMs and, therefore, the identification of potential environmental determinants was based on correlation analysis (see Table S4). Over the southwest Portuguese coast (L7a), no significant (monotonic) relationships were detected between PSP-producers and different environmental variables. At L7c-L8 area, the abundance of PSP-producers was positively correlated with Guadiana and Guadalquivir river discharges, PAR, $I_m$ ($p<0.01$) and Chl-a ($p<0.05$), and negatively correlated with MLD ($p<0.01$). At L9 area, PSP-producers were positively correlated with Guadiana river discharge ($p<0.01$; Table S4).

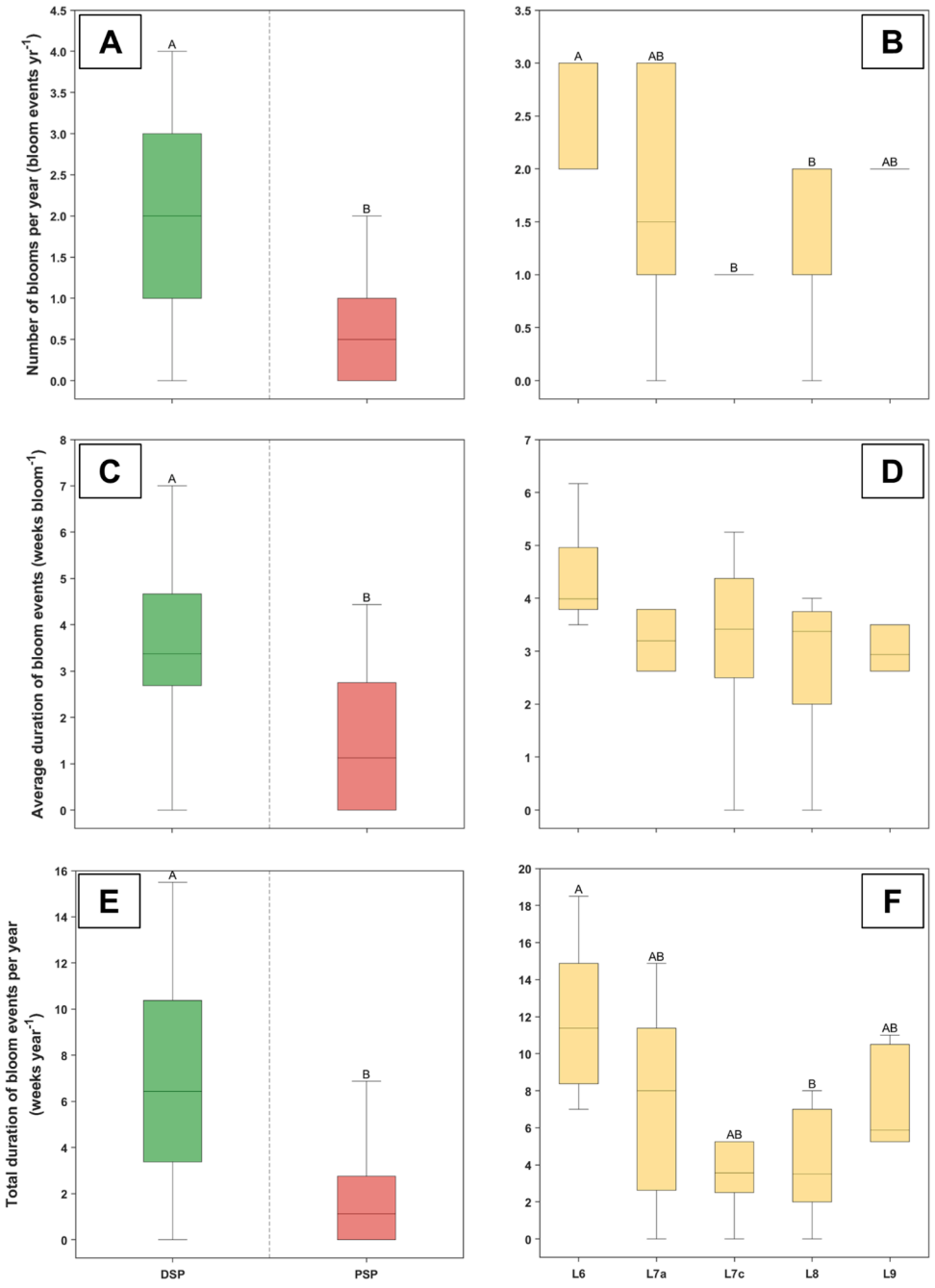


**Fig. 8.** Phytoplankton phenological indices for the three most frequently reported toxin-producing groups (Amnesic Shellfish Poisoning – ASP, Diarrhetic Shellfish Poisoning – DSP, and Paralytic Shellfish Poisoning – PSP, represented by yellow, green, and red colors, respectively), over different shellfish coastal production areas off southern Portugal (L6, L7a, L7c, L8, L9), during the period 2014–2019. The left column includes information for DSP and PSP-producers, aggregated for all coastal production areas (no differences between areas, $p>0.05$), and the right column includes information for ASP-producers, for different coastal production areas. For three phenological indices (bloom initiation timing, bloom peak timing, and peak abundance of ASP-producing species), winter-spring and summer-autumn blooms were considered separately, and represented by dark- and light-yellow colors, respectively. Phenological indices: (A, B) Number of blooms per year; (C, D) Average duration of bloom events; (E, F) Total duration of all bloom events per year; (G, H) Bloom initiation timing; (I, J) Bloom peak timing; and (K, L) Peak abundance of toxin-producing species. Median values are identified by the central line within the box, the bottom and top edges of the box indicate the 25th and 75th percentiles, respectively, and the whiskers represent non-outlier limits. For each phenological index and HAB group, different uppercase letters over the bars denote significant differences across groups (see left column) or coastal productions regions (see right column; $p<0.05$). See Fig. 1 for location of sampling sites and shellfish coastal production areas.

## 4. Discussion

This study, based on a 6-year time series of the abundances of key toxigenic phytoplankton groups, revealed variable intra-annual and phenological patterns in the heterogeneous domain off southern Portugal (e.g., Krug et al., 2017, 2018a, b), depending on HAB-groups and coastal production areas. This variability is consistent with other studies and reinforces the need and value of region- and group-specific HAB studies (e.g., Gianella et al., 2021; Hallegraeff et al., 2021b). Our data on bloom phenology metrics will expand the limited information

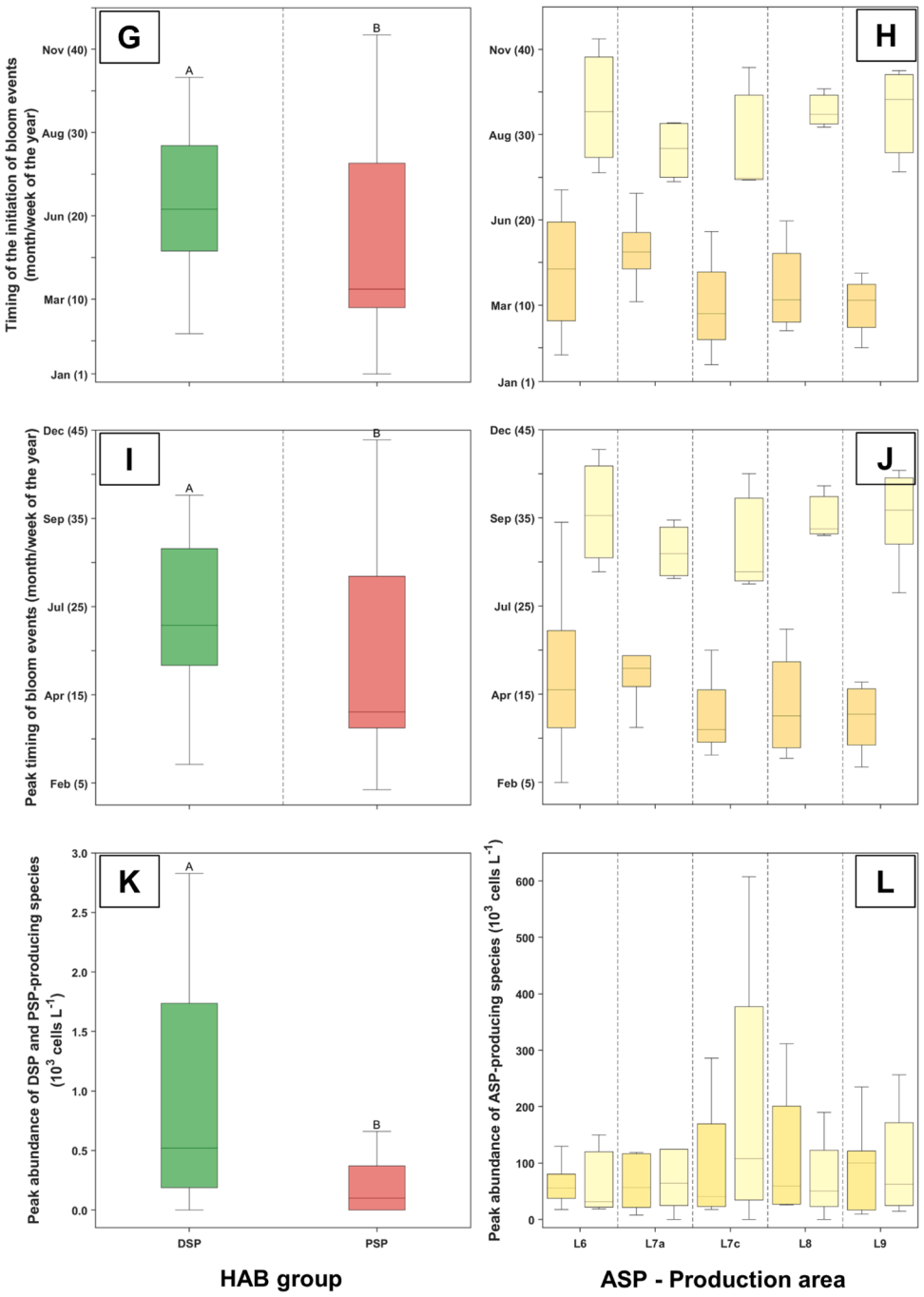


**Fig. 8.** (*continued*).

currently available on HAB phenology (*Alexandrium minutum*: Guallar et al., 2017; *Alexandrium catenella*: Bucci et al., 2020; *Pseudo-nitzschia* spp. and *Phaeocystis globosa*: Karasiewicz and Lefebvre, 2022), particularly relevant in the context of anticipated climate variability and change (Gobler et al., 2017; Wells et al., 2020; Glibert, 2020; Boivin-Rioux et al., 2021, 2022).

This study identified group-specific environmental drivers that may mechanistically affect HABs, either directly or indirectly, and environmental predictors. The latter emerged as influential predictors in empirical-statistical models, reflecting significant statistical relationships, but without necessarily implying any underlying causal relationships (e.g., Ralston and Moore, 2020). In our study, the use of an empirical-statistical flexible cost-effective modeling approach (GAMs) explained 7-8% and 21−54% of the variability in the abundances of ASP- and DSP-producers, respectively, and identified distinct sets of environmental predictors, variable across coastal production areas. Despite relatively reduced predictive skills, further developments of these models (see next subsections), and their integration into hybrid models (see HAB operational forecasting systems: Stumpf et al., 2009; Anderson et al., 2016; Davidson et al., 2021; Fernandes-Salvador et al., 2021), may increase the value of our modelling approach for predicting, and effectively managing HABs over complex coastal domains. Overall, improved comprehensive knowledge on bottom-up and top-down driving forces of specific HAB groups will inevitably expand the list of putative predictors, eventually improving model predictive skills. Future studies should also consider the prediction of toxic events, based on toxin concentration in phytoplankton or living marine resources (e.g., Anderson et al., 2011), which vary depending on the promotors of

**Table 3**
Summary of the best performing generalized additive models (GAMs) used to predict the abundance of toxigenic phytoplankton groups responsible for ASP (Amnesic Shellfish Poisoning) and DSP (Diarrhetic Shellfish Poisoning) human syndromes, for different shellfish coastal production areas off southern Portugal (L7a, L7c-L8, L9), during the period 2014-2019. For each model, information on model explanatory power (MEP), and the significance level of each predictor, in descending order of relevance, are provided. Asterisk symbols *, **, *** indicate p-value <0.05, <0.01 and <0.001, respectively. Along_vel: alongshore current velocity; Chl-a: chlorophyll-a concentration; Gdn: Guadiana river discharge; Gdq: Gualdalquivir river discharge; MLD: mixed layer depth; PAR: surface photosynthetically available radiation; and SST: sea surface temperature. See Fig. 1 for location of coastal production areas, Figs. 9 and 10 for partial effects of individual predictors, and Tables S2-S3 for detailed model statistics.

| HAB taxa | Production Area | MEP (%) | Predictors |
|---|---|---|---|
| ASP | L7a | 6.6 | PAR*** |
| | L7c-L8 | 7.4 | MLD***, SST***, Gdq** |
| | L9 | 7.5 | Along_vel*, Gdn* |
| DSP | L7a | 54 | Chl-a***, MLD***, PAR***, SST** |
| | L7c-L8 | 36 | PAR***, Chl-a***, Gdq**, Along_vel* |
| | L9 | 21 | PAR***, Gdn*, Along_vel* |

phytoplankton toxin production (nutritional, physico-chemical, biological factors; Lelong et al., 2012; Bates et al., 2018; Lewis et al., 2018), and animal detoxification strategies (e.g., Nielsen et al., 2016).

### 4.1. Variability patterns and predictors of ASP-producers

The typically multispecies blooms of ASP-producers, dominated by the diatom genus *Pseudo-nitzschia* (e.g., Trainer et al., 2012; Danchenko et al., 2019; Bresnan et al., 2021; Fernandes-Salvador et al., 2021), represented 41% of all bloom events detected during this study. However, concentrations of ASP-toxins (domoic acid) in bivalve species above the regulatory levels were detected only occasionally (0.5−0.4% samples, at L7c and L9 coastal production areas) during the study period (National Monitoring System of Bivalve Mollusks, IPMA public database; see Table S5). Higher mean and peak abundances of this group, with respect to DSP- and PSP-blooms, probably reflected the high potential *in situ* growth rates of diatoms, an r-strategist opportunistic group (Marañón, 2015; Weithoff and Beisner, 2019). As previously hypothesized, higher abundance of ASP-producers were generally detected over coastal production areas exposed to higher wind and upwelling intensities, along the southwest (L6) and the westernmost sector of the south coast (L7c), with respect to the less exposed L8 and L9 coastal areas (e.g., Relvas and Barton, 2002; see Fig. 2 in Krug et al., 2017, 2018b). In fact, upwelling regimes usually favour diatom growth over other phytoplankton groups (Smayda and Trainer, 2010; Glibert, 2016), specifically species of the genus *Pseudo-nitzschia* (Lelong et al., 2012; Trainer et al., 2012; Bates et al., 2018). The stimulatory effects of upwelling on *Pseudo-nitzschia* blooms can be also magnified when combined with marine heatwaves. During the northeast Pacific marine heatwave, higher temperatures increased *P. australis* growth rate (and northward expansion) and cellular domoic acid, and subsequent nutrient inputs from spring upwelling events were associated with severe blooms along the U.S. west coast (e.g., McCabe et al., 2016; Ryan et al., 2017; Zhu et al., 2017). Yet, the effects of marine heatwaves on toxigenic HABs (e.g., Roberts et al., 2019; Trainer et al., 2020b), may not only result from direct changes on physical-chemical environment, but also from indirect changes on predator activity.

Additionally, high *Pseudo-nitzschia* abundances for the L6 coastal area could also result from the retention of cells leeward of Cape Espichel, which may act as an upwelling shadow area (e.g., Moita et al., 2003; Largier, 2020), or the influence of nutrient-rich discharges from the Sado estuary (Caetano et al., 2016). At L7c area, upwelling induced by local western winds, along with the advection of nutrient-enriched upwelled waters off the southwest coast (e.g., Relvas et al., 2007; Krug et al., 2017) and the cyclonic retentive nearshore circulation patterns (García-Lafuente et al., 2006) may have jointly promoted the abundance of ASP-producers. Despite under high upwelling intensities (see Fig. 2D; Relvas et al., 2007), L7a area revealed the lowest abundances of ASP-producers, along with DSP- and PSP-producers. Over this exposed area, the combined effects of intense coastal upwelling and mesoscale filaments near CSV may be responsible for increased offshore advective transport of *Pseudo-nitzschia* cells and other HAB-producers, as previously referred for phytoplankton (Peliz et al., 2004; Sánchez et al., 2008; Cravo et al., 2010) and crustacean planktonic larval stages (Marta-Almeida et al., 2008; Pires et al., 2013, 2020).

The variable intra-annual patterns of ASP-producers across coastal production areas reflected differences in environmental forcing, ranging from no significant seasonality (L9), a quasi-unimodal cycle with summer maxima (L7a), and bimodal cycles with spring (L7c-L8) or summer maxima (L6). Sustained late winter-spring blooms, usually dominated by diatoms, are commonly referred for temperate coastal and oceanic systems (e.g., Smayda and Trainer, 2010). As reported for phytoplankton blooms in coastal domains of the study area, spring blooms of ASP-producers may have been triggered by increased levels of $I_m$ associated with the MLD shoaling phase (see critical depth hypothesis, Sverdrup, 1953), and additionally supported by early upwelling events, during a stage of well-mixed nutrient-enriched waters (see Krug et al., 2017, 2018b). Yet, later summer blooms of *Pseudo-nitzschia* were probably a result of increased upwelling intensity and nutrient availability. This stimulatory effect of upwelling has been referred for late-spring to late-summer *Pseudo-nitzschia* blooms in Iberian coastal waters (Moita, 2001; Silva et al., 2009; Palma et al., 2010; Vidal et al., 2017; Palenzuela et al., 2019), including the westernmost sector of the south Portuguese coast (Moita, 2001; Loureiro et al., 2005; Danchenko et al., 2019; Santos et al., 2021), and other coastal upwelling systems (see reviews by Trainer et al., 2010 and Pitcher et al., 2017). Higher frequency of relatively short (4-5 weeks, on average; see Table S1) *Pseudo-nitzschia* spp. blooms, detected over L6 and L7a coastal production areas, probably reflected more intense and persistent upwelling-favourable conditions along the southwest coast (e.g., Relvas et al., 2007; see Fig. 2E). An increased phytoplankton bloom frequency was also referred for the southwest Portuguese coast (Krug et al., 2018b), and the occurrence of short frequent *Pseudo-nitzschia* blooms, interrupted by wind-induced, upwelling-relaxation, have also been reported for other coastal upwelling systems (e.g., Smayda and Trainer, 2010; Trainer et al., 2010, 2012; Smith et al., 2018; Palenzuela et al., 2019). Indeed, longer *Pseudo-nitzschia* spp. blooms (bloom length: 246 days, i.e., approximately 30 weeks) were recently reported for coastal areas mostly affected by seasonal stratification-destratification cycles, not shorter upwelling-downwelling cycles (Karasiewicz and Lefebvre, 2022). Interestingly, over L9 coastal production area, subjected to minor upwelling influence and higher riverine discharges, no significant intra-annual patterns in the abundance of ASP-producers were detected, reflecting the complexity of forces acting at the land-ocean interface (Cloern and Jassby, 2008, 2010).

GAM models explained only a small fraction of the variability in the abundance of *Pseudo-nitzschia* spp. during this period (7-8%; see Table 4, for comparison with other studies), and identified multiple (mostly easily accessible) predictors, variable across coastal production areas. In contrast with studies of coastal upwelling systems (Anderson et al., 2009; Pitcher et al., 2010; Du et al., 2016; Smith et al., 2018; Palenzuela et al., 2019), some specifically using empirical-statistical models (Lane et al., 2009; Palma et al., 2010; González Vilas et al., 2014; see Table 4), upwelling intensity was not identified as a significant predictor over the coastal areas most affected by upwelling (L7a, and L7c-L8), only over the L9 coastal area, yet with a low significance level (see Fig. 9). Several processes might have been responsible for the lack of upwelling signature in GAM models of L7a, and L7c-L8 areas. These include the occurrence of other bloom promotors (e.g., spring MLD shallowing), the influence of non-local upwelling events generated along the southwest

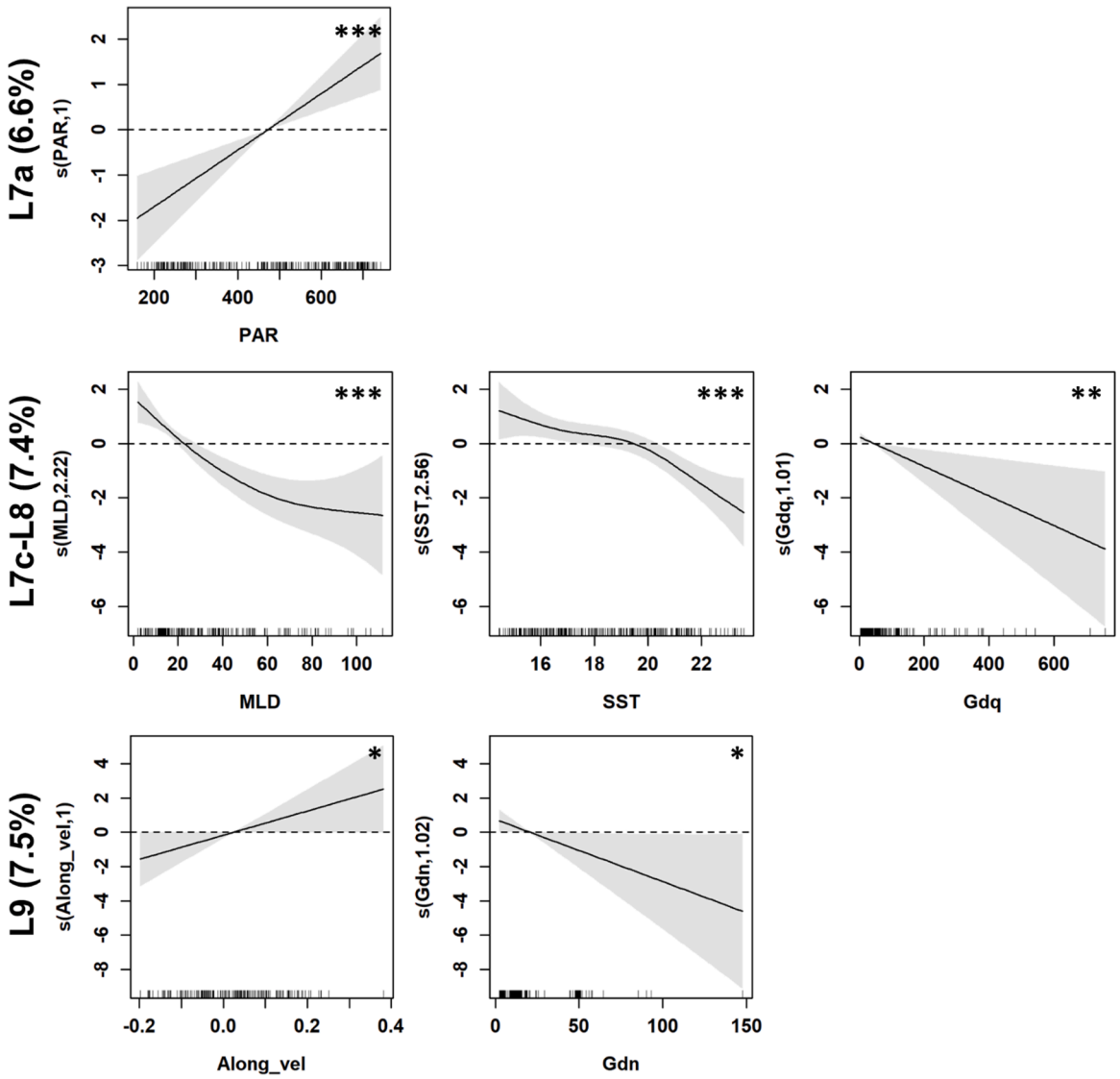


**Fig. 9.** Partial effects of individual environmental predictors on the abundance of Amnesic Shellfish Poisoning (ASP) producers, for each shellfish coastal production area off southern Portugal (L7a, L7c, L8, L9), during the period 2014-2019, derived from the best performing generalized additive models (GAM). Region-specific model explanatory power (as % of ASP variance explained) is presented in brackets, after region abbreviation. For each coastal production area, the set of plots is organized in descending order of their explanatory power, and the significance level (p-value) of each predictor is denoted by asterisk symbols (top right), where *, **, *** indicate p-value <0.05, <0.01 and <0.001, respectively. Solid lines represent the fitted models, and grey shaded areas depict 95% confidence intervals. Short vertical lines on the x-axis represent the actual predictor observations, and values on the y-axis denote the effective degrees of freedom (edf). Edf values of 1 represent a linear effect of the predictor on the abundance of ASP-producers, and values higher than 1 indicate progressively stronger non-linear effects. Positive (negative) y-values indicate a positive (negative) influence on the abundance of ASP producers. See Fig. 1 for location of sampling sites and shellfish coastal production areas.

coast on L7c-L8 areas (e.g., Relvas et al., 2007; Peliz et al., 2007, 2009; Cravo et al., 2010; Goela et al., 2016), increased offshore advection during high intensity upwelling events (e.g., >1000 $m^3\ s^{-1}\ km^{-1}$, Palma et al., 2010; Giddings et al., 2014), differences in surface environmental conditions before upwelling events (e.g., nutrient availability, light; capping of upwelling by riverine plumes, Hickey et al., 2005), and the occurrence of variable time lags between wind-favourable conditions and upwelling events (e.g., Dale et al., 2008), and between upwelling intensification and measurable increases in *Pseudo-nitzschia* abundance (e.g., 4-6 days, Palma et al., 2010; <1-2 weeks, Smith et al., 2018). For example, along the California coast, the uplifting of offshore sub-surface blooms of *Pseudo-nitzschia* during upwelling events quickly seeds surface waters, limiting these time lags (Giddings et al., 2014; Seegers et al., 2015). Further, even if upwelling events are considered a proximate explanation for the stimulation of *Pseudo-nitzschia* spp. growth rate in offshore waters (see Santos et al., 2021), intermittent upwelling relaxation/downwelling events during the upwelling season, that drive shoreward flow, are usually required for accumulation of cells at near-shore sites (Giddings et al., 2014; Hickey et al., 2013; McCabe et al., 2016). These processes can also mask the linkages between upwelling intensity and the response of ASP-producers. Previous studies have also showed that upwelling-related variables, such as SST, PAR, and nutrients can be more important to predict *Pseudo-nitzschia* abundance than wind-derived indices (e.g., Anderson et al., 2010, 2011; Palenzuela et al., 2019; Ajani et al., 2020).

Moreover, the upwelling influence was probably embedded in the set of ASP model predictors. Indeed, GAMs identified positive anomalies in the abundance of ASP-producers (see Fig. 9, and Table 3) for medium-high PAR levels (>500 μmol photons $m^{-2}\ s^{-1}$) over L7a area, and low MLD (<20 m) and low-moderate SST (<20 °C) values over L7c-L8 coastal production areas, environmental conditions that could be considered generally representative of late-spring to summer upwelling

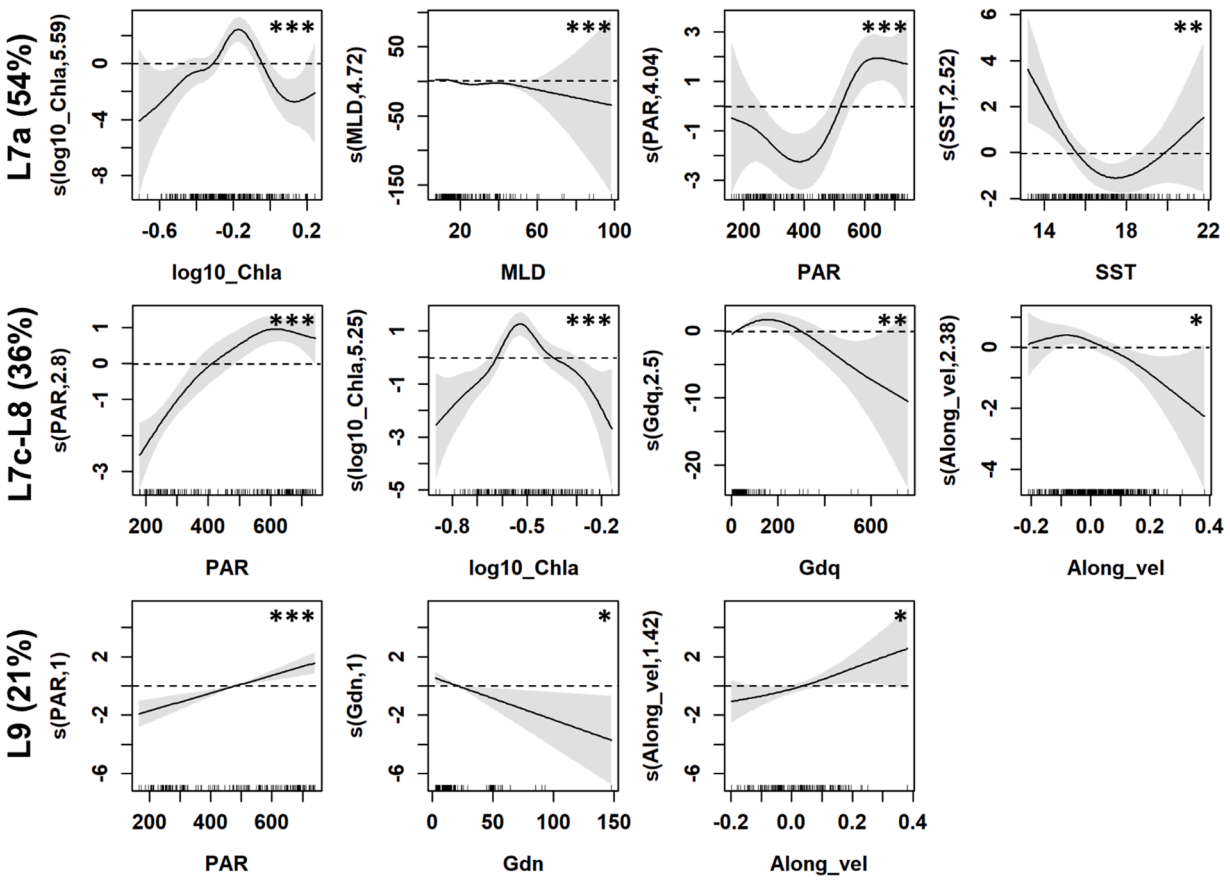


**Fig. 10.** Partial effects of individual environmental predictors on the abundance of Diarrhetic Shellfish Poisoning (DSP) producers, for each shellfish coastal production area off southern Portugal (L7a, L7c, L8, L9), during the period 2014−2019, derived from the best performing generalized additive models (GAM). Region-specific model explanatory power (as % of DSP variance explained) is presented in brackets, after region abbreviation. For each coastal production area, the set of plots is organized in descending order of their explanatory power, and the significance level (*p*-value) of each predictor is denoted by asterisk symbols (top right), where *, **, *** indicate *p*-value <0.05, <0.01 and <0.001, respectively. The solid line is the fitted model and grey shaded areas represent the 95% confidence intervals. The short vertical lines on the x-axis represent the actual predictor observations, and the values on the y-axis denote the effective degrees of freedom (edf). Edf values of 1 represent a linear effect of the predictor on the abundance of DSP-producers, and values higher than 1 indicate progressively stronger non-linear effects. Positive (negative) y-values indicate a positive (negative) influence on the abundance of DSP producers. See Fig. 1 for location of sampling sites and shellfish coastal production areas.

episodes over the later areas (see Krug et al., 2018a). Under replete nutritional conditions, increases in SST from 5 to 28 ºC, depending on the species and strains, can also promote *Pseudo-nitzschia* growth rate, as reported for California (McCabe et al., 2016; Zhu et al., 2017; Kudela et al., 2020). Thus, the negative non-linear effects of SST on *Pseudo-nitzschia* abundance at Lc-L8 coastal area probably reflected the effects of nutrient limiting conditions, generally associated with summer stratified conditions, during upwelling relaxation or downwelling favourable periods (see Krug et al., 2017, 2018a, and references therein). Over coastal production areas along the south coast (L7c-L8 and L9), river discharge was also a predictor of ASP-producers, yet with a lower significance level. River discharge has been proposed as a relevant source of nutrients for phytoplankton in the study area (e.g., Cravo et al., 2006; Caballero et al., 2014; Krug et al., 2017 and references therein; Ferreira et al., 2019), and specifically for *Pseudo-nitzschia* in other coastal systems (Trainer et al., 2012; Bargu et al., 2016; Smith et al., 2018). During high discharge periods (autumn-winter), downwelling favourable conditions and resultant increased alongshore connectivity (Relvas and Barton, 2002; García-Lafuente et al., 2006; Garel et al., 2016) could eventually expand the influence of Guadiana and Guadalquivir river discharges westward (e.g., Hickey et al., 2005), into the sectors west of CSM. However, these potential beneficial effects were not captured by GAMs. The negative linear influence of river discharge could reflect the effects of increased cell advective losses under high discharge rates, increased *Pseudo-nitzschia* sinking rates associated with higher haline stratification (see review Barbosa and Chícharo, 2011), and/or the temporal mismatch between periods of *Pseudo-nitzschia* dominance and high river flow periods, not implying any causal relationship.

The low predictive power of our empirical-statistical models was probably a result of the complexity and variability of driving forces controlling ASP-producers, with local growth and mortality coexisting with intense advective transport of cells from/to non-local sources (e.g., Pitcher et al., 2017; Smith et al., 2018), and the possible occurrence of a high number of species potentially associated with variable ecological niches (see Lelong et al., 2012; Trainer et al., 2012; Bates et al., 2018, and references therein; Lopez et al., 2021). Indeed, over the Portuguese coast, ASP-blooms tend to be dominated by the large *Pseudo-nitzschia seriata*-group during spring, and by the smaller *Pseudo-nitzschia delicatissima*-group during summer (Palma et al., 2010; Santos et al., 2021; Vidal et al., 2017). Moreover, limitations in the sampling strategy, namely the short time series used (6-year), which is not sufficient to detect interannual trends, the relatively low and asynchronous temporal resolution of HAB data (ca. 1 week), which could result in non-detection of very short blooms, the reduced number of stations and their very nearshore location ( beach monitoring; see Anderson et al., 2009), which may not fully represent the conditions associated with the coastal areas, and the areas used for assessing potential environmental predictors can

**Table 4**
Summary of statistical-empirical models used for predicting harmful algal blooms (HAB) for three different toxigenic phytoplankton taxa (I - *Pseudo-nitzschia* spp., II - *Dinophysis* spp., and III - *Gymnodinium catenatum*), with information on the study area and specific target species, model predictors, statistical method used, model predictive power or goodness-of-fit, and associated reference, organized chronologically. Asterisks associated with model references denote hybrid models, that combine empirical-statistical model components with mechanistic-numerical model components. Abbreviations used for model predictors - Chl-a: chlorophyll-a concentration; CSET: cross-shore Ekman transport; MLD: mixed layer depth; NAO: North Atlantic Oscillation; PAR: surface photosynthetically available radiation; SSS: sea surface salinity; and SST: sea surface temperature. Abbreviations used for model methods and predictive power - AUC: Area Under the Curve; MCE: Misclassification Error; NR: Not Referred by the authors; ROC: Receiver Operating Characteristic Curve; SMA: Standardized Major Axis; and TSS: True Skill Statistics.

| Study area *Target HAB*<br>I - *Pseudo-nitzschia* spp. | Predictors | Method | Predictive power/Goodness-of-fit measures | Refs. |
|---|---|---|---|---|
| Santa Barbara Channel (California, USA)<br>*Pseudo-nitzschia* spp. | Remote-sensing reflectance (412-555 nm, 510 nm, 555 nm, 510-555 nm), silicic acid:nitrate, particulate absorption (490 nm), Chl-a | Ordinary Least Squares regression | 53-75% of bloom observations and 93-96% of non-bloom observations | Anderson et al. (2009) |
| Monterey Bay (California)<br>*Pseudo-nitzschia* spp. | Silicic acid, Chl-a, SST, upwelling index, river flow, nitrate | Logistic regression (annual & season-specific) | ≥75% (blooms and non-blooms successfully predicted) | Lane *et al.* (2009) |
| Chesapeake Bay (USA)<br>*Pseudo-nitzschia* spp. | Time of the year, location, phosphate, SST, nitrate plus nitrite, freshwater discharge, salinity, silicic acid, dissolved organic carbon, Secchi depth | Logistic Generalized Linear Model | 0.25 – 0.53 (Heidke Skill Score range) | Anderson *et al.* (2010) |
| Lisbon Bay (west coast, Portugal)<br>*Pseudo-nitzschia* spp. | Upwelling index, SST | Zero-Inflated Generalized Poisson Regression Model | 12 – 36% (estimated proportion of zeros) | Palma *et al.* (2010) |
| Santa Barbara Channel (California, USA)<br>*Pseudo-nitzschia* spp. | Remote-sensing reflectance (510/555 nm), silicic acid to nitrate*nitrite ratio, silicic acid to phosphate ratio, SST, salinity | Logistic Generalized Linear Model | 0.42 – 0.74 (Heidke Skill Score range) | Anderson *et al.* (2011) * |
| Galician rias (northwest coast, Spain)<br>*Pseudo-nitzschia* spp. | Ria, day of the year, SST, salinity, upwelling index, bloom occurrence in previous weeks | Support Vector Machine Model | 0.69 – 0.77 (Kappa value range) | González Vilas *et al.* (2014) |
| Southwest Ireland<br>*Pseudo-nitzschia seriata* and *Pseudo-nitzschia delicatissima* size groups | SST, wind index | Zero-Inflated Negative Binomial Model | 5934.02 (Akaike Information Criteria) | Cusack *et al.* (2015) |
| California coast (USA)<br>*Pseudo-nitzschia* spp. | Remote-sensing reflectance (488/555), month of the year | Logistic Generalized Linear Model | 35 – 43% (accuracy), 35 – 67% (probability of detection), 42 – 67% (false alarm rate), 55 – 83% (probability of false detection), 4 (bias-score), at the corresponding optimized prediction points | Anderson *et al.* (2016) * |
| Alfacs Bay (northwest Mediterranean, Spain)<br>*Pseudo-nitzschia* spp. | Wind velocity, salinity, deep temperature, $\log_{10}$ river flow, $\log_{10}$ atmospheric pressure | Artificial Neural Network | 4 – 15% (MCE), 0.91 – 0.96 (AUC), 0.56 – 0.70 (R-squared) | Guallar *et al.* (2016) |
| Bahía de La Paz (Mexico)<br>*Pseudo-nitzschia* spp. | SST, Chl-a, pH, salinity, dissolved oxygen | Generalized Additive Model | 86% | Matus-Hernández *et al.* (2019)* |
| Galician coast (northwest coast, Spain)<br>*P. delicatissima* and *P. seriata* groups | Salinity, Chl-a, $Si(OH)_4/N$ ratio | Generalized Additive Mixed Model | NR | Palenzuela *et al.* (2019) |
| Hawkesbury River estuary (southeast coast, Australia)<br>*P. delicatissima, P. pungens/multiseries, P. australis/fraudulenta, P. heimii/subpacifica* and *P. americana* groups | Rainfall, SST, turbidity, pH, Chl-a, total abundance cells, soluble reactive phosphorus, total nitrogen, Redfield ratio, week of the year | Generalized Additive Model | 20 – 55% | Ajani *et al.* (2020) |
| Galician Rías Baixas (northwest coast, Spain)<br>*Pseudo-nitzschia* spp. | Day of year, ria code, SST, salinity, bloom occurrence in previous weeks, upwelling indices | Support Vector Machine, Neural Network, Random Forest and AdaBoost | 0.46 – 0.61 (F1-score), 0.32 – 0.58 (distance to the point (0,1) in the ROC curve) | Aláez *et al.* (2021)* |
| Estuary and Gulf of St. Lawrence (east coast, Canada)<br>*P. seriata* | SSS, SST, wind speed | Generalized Additive Model | 0.84 (AUC), 0.54 (TSS) | Boivin-Rioux *et al.* (2022) |
| Off Southern Portugal<br>*Pseudo-nitzschia* spp. | SST, Chl-a, PAR, MLD, river discharge, alongshore current velocity | Generalized Additive Model | 7 – 8% | **This study** |
| II – *Dinophysis* spp. | | | | |
| Bantry Bay (southwest Ireland)<br>*D. acuminata* and *D. acuta* | Wind index, SST | Hydrodynamic and probabilistic models (site-specific) | 0.44 (R-squared) | Raine *et al.* (2010)* |
| Southeastern Arabian Sea (near Mangalore, India)<br>*Dinophysis* spp. | SST, salinity, dissolved inorganic nitrogen to phosphorus ratio, total suspended solids, pH, Secchi depth | Logistic Generalized Linear Model | 0.04 – 0.46 (Heidke Skill Score range) | Singh *et al.* (2014) |
| | Season, thermal stratification, nutrients, salinity, dissolved oxygen | Generalized Additive Model | | Ajani *et al.* (2016) |

(*continued on next page*)

**Table 4** (*continued*)

| | | | | | |
|---|---|---|---|---|---|
| II – *Dinophysis* spp. | | | | | |
| Hawkesbury River (Australia)<br>*D. acuminata* and *D. caudata* | | | | 53% (*D. caudata*), 60% (*D. acuminata*) | |
| Galician Rías Baixas (northwest Iberia)<br>*D. acuta* | NAO index, cumulative upwelling index, SST, tidal range, *D. acuta* inoculum | Generalized Additive Model | | 13 – 77% | Díaz *et al.* (2016) |
| Rías de Aveiro and Pontevedra (northwest coast, Spain)<br>*D. acuminata, D. acuta* | Julian day between 25% percentile and maximum, SST and upwelling index between 25 and 75% percentile, presence/absence of *Dinophysis* cells in water samples during the two previous weeks | Empirical-statistical Model | | 43% (appearance/lack of blooms successfully predicted) | Moita *et al.* (2016) |
| Estuary and Gulf of St. Lawrence (east coast, Canada)<br>*D. acuminata, D. norvegica* | SSS, SST | Generalized Additive Model | | 0.84 – 0.87 (AUC), 0.53 – 0.61 (TSS) | Boivin-Rioux *et al.* (2022) |
| Off Southern Portugal<br>*Dinophysis* spp. | PAR, MLD, SST, Chl-a, river discharge, alongshore current velocity | Generalized Additive Model | | 21 – 54% | **This study** |
| III - *Gymnodinium catenatum* | | | | | |
| Rías Baixas (northwest coast, Spain)<br>*G. catenatum* | NAO index (1 month before the bloom event) | Binary Logistic regression (month-specific) | 75% correctly classified for clearly favourable months and 72% for clearly unfavourable months | | Báez *et al.* (2014) |
| Bahía de La Paz (Mexico)<br>*Gymnodinium* sp. | SST, Chl-a, pH, salinity, dissolved oxygen | Generalized Additive Model | 94% | | Matus-Hernández *et al.* (2019)* |

also explain the low model predictive skills. Future model refinements, assuming the availability of longer, consistent time series, should ideally consider: (i) the discrimination of different groups/species of *Pseudo-nitzschia*; (ii) other potentially relevant predictors, such as the concentration of dissolved inorganic macronutrients, salinity, water column stratification, large-scale climate indices (see Table 4), other upwelling metrics (e.g., cumulative upwelling index, Bograd et al., 2009; wind intermittency, Giddings et al., 2014), and cell concentration (inoculum) in previous periods (see Table 4), tested using variable lag-periods; and (iii) the development of period-specific models, that could identify period-specific predictors (e.g., Lane et al., 2009), some of which could have variable effects on different seasons (e.g., upwelling intensity, river discharge). Also, forthcoming monitoring programs should consider the acquisition of HAB and environmental data using similar spatial and temporal scales.

### 4.2. *Variability patterns and predictors of DSP-producers*

Blooms of DSP-producers represented 43% of all bloom events detected during this study. DSP-toxins (okadaic acid) in bivalves exceed the regulatory levels almost continuously, at all coastal production areas (up to 38% samples, for L8 coastal area), causing recurrent interdictions of bivalve harvesting (National Monitoring System of Bivalve Mollusks, IPMA public database; see Table S5), as reported for other Portuguese systems (e.g., Vale and Sampayo, 2003; Vale et al., 2008; Fernandes-Salvador et al., 2021). These blooms are composed by different species of the genus *Dinophysis* (*D. sacculus, D. caudata, D. fortti*; Bresnan et al., 2021), and usually dominated by *D. acuminata* complex and *D. acuta* over northwestern Iberian shelf (Moita, 2001; Moita et al., 2006a, 2016; Díaz et al., 2016, 2019), and the study area (Goela et al., 2014; Loureiro et al., 2011; Danchenko et al., 2019; Santos et al., 2021). This dinoflagellate group is considered a transitional life-form along the onshore–offshore gradients, more adjusted to less pronounced, smaller-scale convective currents, than *Gymnodinium catenatum* (Smayda and Reynolds, 2001). Contrary to our working hypothesis, similar high mean abundances of *Dinophysis* spp. were detected over coastal production areas exposed to strong wind and upwelling intensities (L6, L7a) and the less exposed L8 area (e.g., Relvas and Barton, 2002; Krug et al., 2017, 2018b). As referred for *Pseudo-nitzschia* spp., lowest abundances detected at L7a coastal area could reflect increased offshore advective losses (see previous subsection).

DSP-producers depicted unimodal annual cycles, with spring-summer maxima, as reported for the study area (Moita, 2001; Santos et al., 2021), and typically referred for dinoflagellates in temperate coastal and oceanic systems. Given their specific set of life traits, including motility, mixotrophy and allelopathy, dinoflagellates are usually well adapted to relatively warm, stratified and nutrient-poor conditions, occurring during this period (Smayda and Trainer, 2010; Glibert and Burford, 2017). Further, *Dinophysis* are obligate kleptoplastidic mixotrophs, thus also depending on the availability of the photosynthetic ciliate *Mesodinium rubrum*, their prey (e.g., Velo-Suárez et al., 2014; Moita et al., 2016; Alves-de-Souza et al., 2019). The spring-summer initiation of *Dinophysis* growth season has been also related with the beginning of the upwelling season, and weak/moderate upwelling events, upwelling relaxation and downwelling events (early autumn transition) have been referred to favour this group in northwestern Iberian shelf waters (Moita et al., 2006a, 2016; Diáz et al., 2016), and southwest Portuguese coastal waters (Loureiro et al., 2005, 2011). Early upwelling events have been hypothesized to introduce a seed (overwintering) population into surface shelf waters, moderate upwelling events can improve the nutritional conditions (e.g., availability of inorganic nutrients, abundance of *M. rubrum*), strong upwelling events were associated with offshore advection of *Dinophysis* (also *M. rubrum*), delaying or eliminating bloom events, and downwelling events (favourable for the encounter of *Dinophysis* and their prey) cause cross-shelf transport and accumulation of *Dinophysis* at nearshore areas

(Reguera et al., 1995; Moita et al., 2006a, 2016; Escalera et al., 2010; Velo-Suárez et al., 2014; Díaz et al., 2013, 2016, 2019; Ruiz-Villarreal et al., 2016). Indeed, in our study, DSP blooms were significantly delayed with respect to ASP winter-spring blooms ($p<0.01$), and were followed by ASP summer-autumn blooms, thus supporting the diatom-dinoflagellate succession associated with upwelling-relaxation cycles in coastal upwelling systems (e.g., Smayda and Trainer, 2010; Trainer et al., 2010, 2012,; Smith et al., 2018; Danchenko et al., 2019).

Despite the effects of alongshore transport of *Dinophysis*, poleward (downwelling) or equatorward (upwelling), observed and/or predicted for northwestern Iberian shelf waters (Díaz et al., 2013; Moita et al., 2016; Ruiz-Villarreal et al., 2016), onset and peak timings of DSP-blooms were *quasi*-synchronous across all coastal production areas. The use of only very nearshore stations in this study limited further analysis of the relevance of cross-shore and alongshore processes. Moreover, our results represent the responses of all *Dinophysis* species combined, not allowing the detection of inter-specific differences, such as those reported for *D. acuminata* (earlier surface blooms) and *D. acuta* (later sub-surface blooms; Vale and Sampayo, 2003; Escalera et al., 2006, 2010; Reguera et al., 2012, Moita et al., 2016; Díaz et al., 2019). These differences would probably lead to higher bloom frequency, shorter bloom events, and a departure from unimodal annual cycles.

GAMs explained a higher fraction of the variability in the abundance of *Dinophysis* spp. (21−54%), when compared with ASP-models, within the range of values reported by other studies (see Table 4). In addition to the study limitations and improvements suggested for ASP-models (see subsection 4.1), forthcoming development of DSP-models should consider species-specific models (see *D. acuminata versus D. acuta*, Moita et al., 2016), and period-specific models or variables (see Díaz et al., 2016), and the inclusion of additional potential predictors (see Table 4), including turbulence, thermal stratification, and the abundance of *Mesodinium rubrum*. Overall, considering the most relevant predictors (see Fig. 10 and Table 3), positive anomalies in the abundance of *Dinophysis* spp. were detected for medium-high PAR levels (>400−500 μmol photons $m^{-2}$ $s^{-1}$), for all coastal production areas, intermediate Chl-a (0.2 - 0.6 μg $L^{-1}$; L7a and L7c-L8 areas), and low MLD (<20m; L7a area). This window of opportunity generally reflected the environmental conditions (stratified, nutrient-poor) associated with *Dinophysis* intra-annual patterns (spring-summer maxima), in the study area, (e.g., Krug et al., 2017, 2018a), that favour dinoflagellates over diatoms (Glibert and Burford, 2017).

Over the coastal production areas located along the south coast (L7c-L8 and L9), upwelling patterns and river discharge were also significant, yet less influential predictors of *Dinophysis* abundance (see Fig. 10 and Table 3). The modest and contrasting partial effects of upwelling/downwelling-favourable conditions (negative and positive effects of upwelling for L7c-L8, and L9 areas, respectively), probably reflected the complex responses of this group to upwelling patterns (e.g., Pitcher et al., 2017), as previously discussed for ASP-producers (see previous subsection). For longer time series, the development of period-specific models (e.g., upwelling season; Loureiro et al., 2011) could probably clarify the influence of upwelling as a *Dinophysis* predictor (Díaz et al., 2016). Moreover, the negative anomalies of *Dinophysis* associated with high river discharges probably reflected increased advective losses (e.g., Moita et al., 2016), as also referred for *Pseudo-nitzschia*. Yet, modest positive anomalies associated with low to medium river discharges could point to their beneficial effects on *Dinophysis*, associated with increases in nutrient availability (Cravo et al., 2006; Caballero et al., 2014; Correia et al., 2020), mainly during downwelling periods (see Hickey et al., 2005), decreased turbulence and increased $I_m$, due to haline stratification (e.g., Peperzak et al., 1996; Díaz et al., 2013, 2021; Moita et al., 2016).

### 4.3. Variability patterns and predictors of PSP-producers

Blooms of PSP-producers represented a minor fraction (16%) of the bloom events detected, and PSP-toxins (saxitoxins) in bivalves exceeded the regulatory levels occasionally (0.3−5.0% samples) during the study period (National Monitoring System of Bivalve Mollusks, IPMA public database; see Table S5). Indeed, these blooms are relatively less recurrent in Portuguese waters (see Costa et al., 2010; Vale, 2013; Botelho et al., 2019). Blooms of PSP-producers are composed by different species of dinoflagellates (*Alexandrium minutum, Gymnodinium catenatum*; Bresnan et al., 2021), but usually dominated by *G. catenatum* in the westernmost sector of the south Portuguese coast (Loureiro et al., 2011; Danchenko et al., 2019), and over northwestern Iberian shelf waters (Sordo et al., 2001; Moita et al., 2006b; Bravo et al., 2010). As previously hypothesized and, in contrast with ASP-producers, lower mean abundances of PSP-producers were detected over coastal production areas exposed to higher wind and upwelling intensity (L6 and L7a), probably reflecting increased offshore advection (Moita et al., 1998), and higher competitive advantage of diatoms over dinoflagellates for these areas (Pitcher et al., 2010; Smayda, 2010).

The reduced number of samples with non-zero abundances, namely during the period 2016-2019, associated with shorter less frequent blooms, constrained our analysis of variability patterns and environmental determinants of PSP-producers. Overall, this group showed complex variability patterns, with maximum abundances mostly detected between early-spring and mid-summer, generally classified as an upwelling-favourable period (e.g., Relvas et al., 2007), but still affected by several alternating upwelling-downwelling episodes. *G. catenatum* blooms have been mostly associated with upwelling relaxation or downwelling conditions (early autumn) for the study area (Loureiro et al., 2011; Danchenko et al., 2019), and northwestern Iberian shelf waters (Fraga et al., 1988; Tilstone et al., 1994; Moita, 2001; Sordo et al., 2001; Bravo et al., 2010; Moita et al., 2003; Díaz et al., 2019). Notwithstanding the occurrence of *Gymnodinium catenatum* cysts in shelf sediments (Amorim et al., 2001, 2004), PSP-blooms off Iberia apparently develop from offshore "pelagic seed banks" (Moita et al., 1998; Amorim et al., 2004; Loureiro et al., 2011), that are advected onshore during upwelling relaxation or downwelling periods, and further transported alongshore depending on the predominant wind patterns (Sordo et al., 2001; Bravo et al., 2010) or concentrated at highly retentive areas (e.g., upwelling fronts, upwelling shadow areas; Moita et al., 2003). In fact, this mixotrophic species (Jeong et al., 2005) is considered an upwelling relaxation life-form (Smayda and Reynolds, 2010), with functional traits (e.g., tolerance to elevated shear stress, high swimming rate and vertical migration, chain formation) of high adaptive value under upwelling relaxation or downwelling conditions (e.g., Smayda, 2010; Smayda and Reynolds, 2010; Hallegraeff et al., 2012). Further, over the coastal production areas along the south coast (L7c-L8 and L9), positive relationships between the abundance of *G. catenatum* and river discharges probably reflected the fertilizing effect of nutrient-rich waters (Hallegraeff et al., 1995, 2012), over a coastal domain more stratified and less exposed to upwelling patterns (see Krug et al., 2017, 2018a). Indeed, high nutrient concentrations have been reported for the lower Guadiana estuary (see Correia et al., 2020 and references therein), and Guadalquivir estuarine plume (Prieto et al., 2009; Ribas-Ribas et al., 2013). In comparison with other HAB groups, advective flushing of *G. catenatum* under high riverine discharges was apparently minimized. Higher affinity for turbulence, chain formation, and strong motility allow this dinoflagellate species to undergo vertical migration and explore highly dynamic environments (Smayda and Reynolds, 2001; Hallegraeff et al., 2012).

## 5. Conclusions

The present study contributed to a better understanding of HABs spatial-temporal variability patterns, phenology, and associated environmental drivers and predictors in the heterogenous coastal waters off southern Portugal. Our data on bloom phenology metrics will expand the limited information currently available for toxigenic phytoplankton,

particularly relevant in the context of anticipated climate changes. As hypothesized, *Pseudo-nitzschia* spp. blooms were more frequently observed in coastal areas under stronger upwelling intensity (southwest coast, and westernmost sector of the south coast), while *G. catenatum* (occasional) blooms prevailed in areas more influenced by river discharges, under weaker upwelling (southeastern coast). *Pseudo-nitzschia* spp. mostly presented spring and summer maxima, reflecting firstly the influence of increased light intensity during the MLD shoaling stage, and later the stimulatory effects of upwelling events. *Dinophysis* spp. showed spring/summer maxima, under environmental conditions that typically promote dinoflagellate development, and connections with the oceanographic regime (upwelling-downwelling) were not clearly discernible. In contrast with *Dinophysis*, positive linkages between *G. catenatum* and river discharge probably reflected adaptative traits more adjusted to highly dynamic environments, emphasizing the variability within dinoflagellates. Blooms of *Pseudo-nitzschia* spp. were more intense than dinoflagellate blooms, and bloom onset and peak timings also differed between groups. Delayed *Dinophysis* spp. blooms with respect to *Pseudo-nitzschia* spp. spring blooms, followed by *Pseudo-nitzschia* spp. summer blooms, probably reflected the dynamics of upwelling-relaxation cycles over the study area.

GAMs, a flexible cost-effective statistical-empirical modeling approach applied here for *Pseudo-nitzschia* spp. and *Dinophysis* spp., presented low to moderate explanatory power, higher for the latter group (21-54%), responsible for the majority of HAB events and bivalve harvesting interdictions in the study area. Easily accessed environmental variables, PAR, MLD, SST, and Chl-a, were the most influential predictors, and river discharges showed minor negative effects over both HAB groups for the coastal production areas along the south coast. Despite several lines of evidence supporting the role of upwelling as an environmental driver of *Pseudo-nitzschia* spp., upwelling intensity was not identified as a relevant model predictor. In this context, this study encourages the use of these two concepts, environmental drivers and environmental predictors, separately and independently, rather than as synonyms. Future model developments should consider species-specific and period-specific models, and other environmental predictors, including both bottom-up and top-down controls (e.g., inorganic nutrients, salinity, stratification, turbulence intensity, prey abundance for mixotrophic harmful taxa, grazing), thus reinforcing the need to improve current HAB monitoring programs. The integration of enhanced empirical-statistical models into hybrid modelling approaches may further support the implementation of HAB operational forecasting systems, and effective HAB management programs over complex coastal domains.

## Declaration of Competing Interest

The authors declare that they have no known competing financial interests or personal relationships that could have appeared to influence the work reported in this paper.

## Acknowledgments

This work is a contribution of the project MAR-01.04.02-FEAMP-0003, “Contributo para a Proteção do recurso amêijoa *Ruditapes decussatus* no ecossistema da Ria Formosa. Diagnóstico ambiental nas áreas de influência das estações de tratamento de águas residuais urbanas”, funded by Programa Operacional Mar 2020, Fundo Europeu dos Assuntos Marítimos e das Pescas (FEAMP). M.J.L was also supported by this research. The authors wish also to express their gratitude to Instituto Português do Mar e da Atmosfera, IPMA (abundance of toxigenic phytoplankton and biotoxin concentration in selected bivalve species), European Space Agency (ESA)’s OC-CCI group (chlorophyll-a), NASA’s Oceancolor database (sea surface temperature, and photosynthetically available radiation data), Ocean Productivity (mixed layer depth), Copernicus Marine Service (mixed layer depth, and wind data), NOAA’s National Centres for Environmental Information (wind data), Agência Portuguesa do Ambiente (Guadiana river discharge data), and Sistema Automático de Información Hidrológica (Guadalquivir river discharge data) for providing free, regular, and high-quality products to the scientific community. The authors would also like to thank Dr Erwan Garel (CIMA) for giving access to alongshore current velocity data, and acknowledge the financial support of Fundação para a Ciência e Tecnologia to Centro de Investigação Marinha e Ambiental (CIMA-Universidade do Algarve), through grant UIDP/00350/2020. The authors sincerely thank anonymous reviewers for the valuable comments that improved the quality of the manuscript.

## Supplementary materials

Supplementary material associated with this article can be found, in the online version, at doi:10.1016/j.hal.2022.102254.

## References

Ajani, P., Larsson, M.E., Rubio, A., Bush, S., Brett, S., Farrell, H., 2016. Modelling bloom formation of the toxic dinoflagellates *Dinophysis acuminata* and *Dinophysis caudata* in a highly modified estuary, south eastern Australia. Estuar. Coast. Shelf Sci. 183, 95–106. https://doi.org/10.1016/j.ecss.2016.10.020.

Ajani, P.A., Larsson, M.E., Woodcock, S., Rubio, A., Farrell, H., Brett, S., Murray, S.A., 2020. Fifteen years of *Pseudo-nitzschia* in an Australian estuary, including the first potentially toxic *P. delicatissima* bloom in the southern hemisphere. Estuar. Coast. Shelf Sci. 236, 106651 https://doi.org/10.1016/j.ecss.2020.106651.

Aláez, F.M.B., Palenzuela, J.M.T., Spyrakos, E., Vilas, L.G., 2021. Machine Learning Methods Applied to the Prediction of *Pseudo-nitzschia* spp. Blooms in the Galician Rias Baixas (NW Spain). ISPRS. Int. J. Geo Inf. 10 https://doi.org/10.3390/ijgi10040199.

Alvarez, I., Gomez-Gesteira, M., DeCastro, M., Lorenzo, M., Crespo, A., Dias, J., 2011. Comparative analysis of upwelling influence between the western and northern coast of the Iberian Peninsula. Cont. Shelf Res. 31, 388–399. https://doi.org/10.1016/j.csr.2010.07.009.

Alves-de-Souza, C., Iriarte, J.L., Mardones, J.I., 2019. Interannual Variability of *Dinophysis acuminata* and *Protoceratium reticulatum* in a Chilean Fjord: insights from the realized niche analysis. Toxins 11 (1), 1–23. https://doi.org/10.3390/toxins11010019.

Amorim, A., Dale, B., Godinho, R., Brotas, V., 2001. *Gymnodinium catenatum*-like cysts (Dinophyceae) in recent sediments from the coast of Portugal. Phycologia 40, 572–582. https://doi.org/10.2216/i0031-8884-40-6-572.1.

Amorim, A., Moita, M.T., Oliveira, P., 2004. Dinoflagellate blooms related to coastal upwelling plumes off Portugal. Harmful Algae 89–91.

Anderson, C.R., Sapiano, M.R.P., Prasad, M.B.K., Long, W., Tango, P.J., Brown, C.W., Murtugudde, R., 2010. Predicting potentially toxigenic *Pseudo-nitzschia* blooms in the Chesapeake Bay. J. Mar. Syst. 83, 127–140. https://doi.org/10.1016/j.jmarsys.2010.04.003.

Anderson, C.R., Kudela, R.M., Benitez-Nelson, C., Sekula-Wood, E., Burrell, C.T., Chao, Y., Langlois, G., Goodman, J., Siegel, D.A., 2011. Detecting toxic diatom blooms from ocean color and a regional ocean model. Geophys. Res. Lett. 38, L04603. https://doi.org/10.1029/2010GL045858.

Anderson, C.R., Kudela, R.M., Kahru, M., Chao, Y., Rosenfeld, L.K., Bahr, F.L., Anderson, D.M., Norris, T.A., 2016. Initial skill assessment of the California Harmful Algae Risk Mapping (C-HARM) system. Harmful Algae 59, 1–18. https://doi.org/10.1016/j.hal.2016.08.006.

Anderson, D., 2009. Approaches to monitoring, control and management of harmful algal blooms (HABs). Ocean Coast. Manag. 52, 342–347. https://doi.org/10.1016/j.ocecoaman.2009.04.006.

Anderson, D.M., Cembella, A.D., Hallegraeff, G.M., 2012. Progress in understanding harmful algal blooms: paradigm shifts and new technologies for research, monitoring, and management. Ann. Rev. Mar. Sci. 4, 143–176. https://doi.org/10.1146/annurev-marine-120308-081121.

Anderson, D.M., Fensin, E., Gobler, C.J., Hoeglund, A.E., Hubbard, K.A., Kulis, D.M., Landsberg, J.H., Lefebvre, K.A., Provoost, P., Richlen, M.L., Smith, J.L., Solow, A.R., Trainer, V.L., 2021. Marine harmful algal blooms (HABs) in the United States: history, current status and future trends. Harmful Algae 102, 101975. https://doi.org/10.1016/j.hal.2021.101975.

Arístegui, J., Barton, E.D., Álvarez-Salgado, X.A., Santos, A.M.P., Figueiras, F.G., Kifani, S., Hernández-León, S., Mason, E., Machú, E., Demarcq, H., 2009. Sub-regional ecosystem variability in the Canary Current upwelling. Prog. Oceanogr. 83, 33–48. https://doi.org/10.1016/j.pocean.2009.07.031.

Báez, J.C., Real, R., López-Rodas, V., Costas, E., Salvo, A.E., García-Soto, C., Flores-Moya, A., 2014. The North Atlantic Oscillation and the Arctic Oscillation favour harmful algal blooms in SW Europe. Harmful Algae 39, 121–126. https://doi.org/10.1016/j.hal.2014.07.008.

Bakun, A., 1973. Coastal Upwelling Indices. West Coast of North America, pp. 1946–1971.

Barbosa, A.B., Chícharo, M.A., 2011. Hydrology and Biota Interactions as Driving Forcesfor Ecosystem Functioning. Elsevier (Eds.). In: Wolanski, E., McLusky, D.S.

(Eds.), Treatise on Estuarine and Coastal Science. Ecohydrology and Restoration, pp. 7–47. Volume 10.
Bargu, S., Baustian, M.M., Rabalais, N.N., Del Rio, R., Von Korff, B., Turner, R.E., 2016. Influence of the Mississippi River on *Pseudo-nitzschia* spp. Abundance and toxicity in Louisiana coastal waters. Estuar. Coasts 39, 1345–1356. https://doi.org/10.1007/s12237-016-0088-y.
Barton, A.D., Finkel, Z.V, Ward, B.A., Johns, D.G., Follows, M.J., 2013. On the roles of cell size and trophic strategy in North Atlantic diatom and dinoflagellate communities. Limnol. Oceanogr. 58, 254–266. https://doi.org/10.4319/lo.2013.58.1.0254.
Bates, S., Hubbard, K., Lundholm, N., Montresor, M., Leaw, C., 2018. *Pseudo-nitzschia, Nitzschia*, and domoic acid: new research since 2011. Harmful Algae 79, 3–43. https://doi.org/10.1016/j.hal.2018.06.001.
Behrenfeld, M.J., Doney, S.C., Lima, I., Boss, E.S., Siegel, D.A., 2013. Annual cycles of ecological disturbance and recovery underlying the subarctic Atlantic spring plankton bloom. Glob. Biogeochem. Cycles 27, 526–540. https://doi.org/10.1002/gbc.20050.
Belin, C., Soudant, D., Amzil, Z., 2021. Three decades of data on phytoplankton and phycotoxins on the French coast: lessons from REPHY and REPHYTOX. Harmful Algae 102, 101733. https://doi.org/10.1016/j.hal.2019.101733.
Berdalet, E., Fleming, L.E., Gowen, R., Davidson, K., Hess, P., Backer, L.C., Moore, S.K., Hoagland, P., Enevoldsen, H., 2016. Marine harmful algal blooms, human health and wellbeing: challenges and opportunities in the 21st century. J. Mar. Biol. Assoc. UK 96, 61–91. https://doi.org/10.1017/S0025315415001733.
Bograd, S.J., Schroeder, I., Sarkar, N., Qiu, X., Sydeman, W.J., Schwing, F.B., 2009. Phenology of coastal upwelling in the California current. Geophys. Res. Lett. 36, 1–5. https://doi.org/10.1029/2008GL035933.
Boivin-Rioux, A., Starr, M., Chassé, J., Scarratt, M., Perrie, W., Long, Z., 2021. Predicting the effects of climate change on the occurrence of the toxic dinoflagellate *Alexandrium catenella* along Canada's East Coast. Front. Mar. Sci. 7, 1–20. https://doi.org/10.3389/fmars.2020.608021.
Boivin-Rioux, A., Starr, M., Chassé, J., Scarratt, M., Perrie, W., Long, Z., Lavoie, D., 2022. Harmful algae and climate change on the Canadian East Coast: exploring occurrence predictions of *Dinophysis acuminata, D. norvegica*, and *Pseudo-nitzschia seriata*. Harmful Algae 112, 102183. https://doi.org/10.1016/j.hal.2022.102183.
Botelho, M.J., Vale, C., Ferreira, J.G., 2019. Seasonal and multi-annual trends of bivalve toxicity by PSTs in Portuguese marine waters. Sci. Total Environ. 664, 1095–1106. https://doi.org/10.1016/j.scitotenv.2019.01.314.
Bravo, I., Fraga, S., Isabel Figueroa, R., Pazos, Y., Massanet, A., Ramilo, I., 2010. Bloom dynamics and life cycle strategies of two toxic dinoflagellates in a coastal upwelling system (NW Iberian Peninsula). Deep Sea Res. Part II Top. Stud. Oceanogr. 57, 222–234. https://doi.org/10.1016/j.dsr2.2009.09.004.
Bresnan, E., Arévalo, F., Belin, C., Branco, M.A.C., Cembella, A.D., Clarke, D., Correa, J., Davidson, K., Dhanji-Rapkova, M., Lozano, R.F., Fernández-Tejedor, M., Guðfinnsson, H., Carbonell, D.J., Laza-Martinez, A., Lemoine, M., Lewis, A.M., Menéndez, L.M., Maskrey, B.H., McKinney, A., Pazos, Y., Revilla, M., Siano, R., Silva, A., Swan, S., Turner, A.D., Schweibold, L., Provoost, P., Enevoldsen, H., 2021. Diversity and regional distribution of harmful algal events along the Atlantic margin of Europe. Harmful Algae 102, 101976. https://doi.org/10.1016/j.hal.2021.101976.
Brown, C.W., Hood, R.R., Long, W., Jacobs, J., Ramers, D.L., Wazniak, C., Wiggert, J.D., Wood, R., Xu, J., 2013. Ecological forecasting in Chesapeake Bay: using a mechanistic–empirical modeling approach. J. Mar. Syst. 125, 113–125. https://doi.org/10.1016/j.jmarsys.2012.12.007.
Bucci, A.F., Thomas, A.C., Cetinić, I., 2020. Interannual variability in the thermal habitat of Alexandrium Catenella in the Bay of Fundy and the implications of climate change. Front. Mar. Sci. 7, 1–15. https://doi.org/10.3389/fmars.2020.587990.
Caballero, I., Morris, E., Pietro, L., Navarro, G., 2014. The influence of the Guadalquivir River on the spatio-temporal variability of suspended solids and chlorophyll in the Eastern Gulf of Cadiz. Mediterr. Mar. Sci. 15, 721–738. https://doi.org/10.12681/mms844.
Caballero, I., Fernández, R., Escalante, O.M., Mamán, L., Navarro, G., 2020. New capabilities of Sentinel-2A/B satellites combined with in situ data for monitoring small harmful algal blooms in complex coastal waters. Sci. Rep. 10, 1–14. https://doi.org/10.1038/s41598-020-65600-1.
Caetano, M., Raimundo, J., Nogueira, M., Santos, M., Mil-Homens, M., Prego, R., Vale, C., 2016. Defining benchmark values for nutrients under the Water Framework Directive: application in twelve Portuguese estuaries. Mar. Chem. 185, 27–37. https://doi.org/10.1016/j.marchem.2016.05.002.
Cloern, J.E., Jassby, A.D., 2008. Complex seasonal patterns of primary producers at the land-sea interface. Ecol. Lett. 11, 1294–1303. https://doi.org/10.1111/j.1461-0248.2008.01244.x.
Cloern, J.E., Jassby, A.D., 2010. Patterns and scales of phytoplankton variability in estuarine – coastal ecosystems. Estuar. Coasts 33, 230–241. https://doi.org/10.1007/s12237-009-9195-3.
Cloern, J.E., Foster, S.Q., Kleckner, A.E., 2014. Phytoplankton primary production in the world's estuarine-coastal ecosystems. Biogeosciences 11, 2477–2501. https://doi.org/10.5194/bg-11-2477-2014.
Correia, C., Torres, A.F., Rosa, A., Cravo, A., Jacob, J., de Oliveira Júnior, L., Garel, E., 2020. Export of dissolved and suspended matter from the main estuaries in South Portugal during winter conditions. Mar. Chem. 224, 103827 https://doi.org/10.1016/j.marchem.2020.103827.
Costa, P.R., Botelho, M.J., Lefebvre, K.A., 2010. Characterization of paralytic shellfish toxins in seawater and sardines (*Sardina pilchardus*) during blooms of *Gymnodinium catenatum*. Hydrobiologia 655, 89–97. https://doi.org/10.1007/s10750-010-0406-5.
Cravo, A., Madureira, M., Felícia, H., Rita, F., Bebianno, M.J., 2006. Impact of outflow from the Guadiana River on the distribution of suspended particulate matter and nutrients in the adjacent coastal zone. Estuar. Coast. Shelf Sci. 70, 63–75. https://doi.org/10.1016/j.ecss.2006.05.034.
Cravo, A., Relvas, P., Cardeira, S., Rita, F., Madureira, M., Sánchez, R., 2010. An upwelling filament off southwest Iberia: Effect on the chlorophyll a and nutrient export. Cont. Shelf Res. 30, 1601–1613. https://doi.org/10.1016/j.csr.2010.06.007.
Cravo, A., Barbosa, A.B., Correia, C., Matos, A., Caetano, S., Lima, M.J., Jacob, J., 2022. Unravelling the effects of treated wastewater discharges on the water quality in a coastal lagoon system (Ria Formosa, South Portugal): relevance of hydrodynamic conditions. Mar. Pollut. Bull. 174, 113296 https://doi.org/10.1016/j.marpolbul.2021.113296.
Cristina, S., Cordeiro, C., Lavender, S., Costa Goela, P., Icely, J., Newton, A., 2016. MERIS phytoplankton time series products from the SW Iberian Peninsula (Sagres) using seasonal-trend decomposition based on loess. Remote Sens. 8 (6), 449. https://doi.org/10.3390/rs8060449.
Cruz, R.C., Reis Costa, P., Vinga, S., Krippahl, L., Lopes, M.B., 2021. A review of recent machine learning advances for forecasting harmful algal blooms and shellfish contamination. J. Mar. Sci. Eng. 9 (3), 283. https://doi.org/10.3390/jmse9030283.
Cusack, C., Mouriño, H., Moita, M.T., Silke, J., 2015. Modelling *Pseudo-nitzschia* events off southwest Ireland. J. Sea Res. 105, 30–41. https://doi.org/10.1016/j.seares.2015.06.012.
Dale, A.C., Barth, J.A., Levine, M.D., Austin, J.A., 2008. Observations of mixed layer restratification by onshore surface transport following wind reversal in a coastal upwelling region. J. Geophys. Res. Ocean. 113 https://doi.org/10.1029/2007JC004128.
Danchenko, S., Fragoso, B., Guillebault, D., Icely, J., Berzano, M., Newton, A., 2019. Harmful phytoplankton diversity and dynamics in an upwelling region (Sagres, SW Portugal) revealed by ribosomal RNA microarray combined with microscopy. Harmful Algae 82, 52–71. https://doi.org/10.1016/j.hal.2018.12.002.
Davidson, K., Whyte, C., Aleynik, D., Dale, A., Gontarek, S., Kurekin, A.A., McNeill, S., Miller, P.I., Porter, M., Saxon, R., Swan, S., 2021. HABreports: online early warning of harmful algal and biotoxin risk for the Scottish shellfish and finfish aquaculture industries. Front. Mar. Sci. 8, 631732 https://doi.org/10.3389/fmars.2021.631732.
De Oliveira Júnior, L., Garel, E., Relvas, P., 2021. The structure of incipient coastal counter currents in South Portugal as indicator of their forcing agents. J. Mar. Syst. 214, 103486 https://doi.org/10.1016/j.jmarsys.2020.103486.
Díaz, P.A., Reguera, B., Ruiz-Villarreal, M., Pazos, Y., Velo-Suárez, L., Berger, H., Sourisseau, M., 2013. Climate variability and oceanographic settings associated with interannual variability in the initiation of *Dinophysis acuminata* blooms. Mar. Drugs 11 (8), 2964–2981. https://doi.org/10.3390/md11082964.
Díaz, P.A., Ruiz-villarreal, M., Pazos, Y., Moita, T., Reguera, B., 2016. Climate variability and *Dinophysis acuta* blooms in an upwelling system. Harmful Algae 53, 145–159. https://doi.org/10.1016/j.hal.2015.11.007.
Díaz, P., Reguera, B., Moita, T., Bravo, I., Ruiz-Villarreal, M., Fraga, S., 2019. Mesoscale dynamics and niche segregation of two *Dinophysis* species in Galician-Portuguese coastal waters. Toxins (Basel) 11, 1–21. https://doi.org/10.3390/toxins11010037.
Dormann, C.F., Elith, J., Bacher, S., Buchmann, C., Carl, G., Carré, G., García Marquéz, J. R., Gruber, B., Lafourcade, B., Leitão, P.J., Munkemuller, T., Mcclean, C., Osborne, P. E., Reineking, B., Schroder, B., Skidmore, A.K., Zurell, D., Lautenbach, S., 2013. Collinearity: a review of methods to deal with it and a simulation study evaluating their performance. Ecography (Cop.) 36, 27–46. https://doi.org/10.1111/j.1600-0587.2012.07348.x.
Du, X., Peterson, W., Fisher, J., Hunter, M., Peterson, J., 2016. Initiation and development of a toxic and persistent *Pseudo-nitzschia* bloom off the Oregon coast in spring/summer 2015. PLoS One 11, 1–17. https://doi.org/10.1371/journal.pone.0163977.
Dunn, O.J., 1961. Multiple comparisons among means. J. Am. Stat. Assoc. 56, 52–64. https://doi.org/10.1080/01621459.1961.10482090.
EC, 2004a. Regulation (EC) No. 853/2004 of the European Parliament and of the Council of 29 April 2004, laying down hygiene rules for on the hygiene of foodstuffs. Official Journal of the European Union L 139 47, 55–205.
EC, 2004b. Regulation (EC) No. 854/2004 of the European Parliament and of the Council of 29 April 2004, laying down specific rules for the organisation of official controls on products of animal origin intended for human consumption. Official Journal of the European Union L 139 47, 206–320.
Escalera, L., Reguera, B., Pazos, Y., Moroño, A., Cabanas, J.M., 2006. Are different species of *Dinophysis* selected by climatological conditions? Afr. J. Mar. Sci. 28, 283–288. https://doi.org/10.2989/18142320609504163.
Escalera, L., Reguera, B., Moita, T., Pazos, Y., Cerejo, M., Cabanas, J.M., Ruiz-Villarreal, M., 2010. Bloom dynamics of *Dinophysis* acuta in an upwelling system: *in situ* growth versus transport. Harmful Algae 9, 312–322. https://doi.org/10.1016/j.hal.2009.12.002.
Falkowski, P.G., Barber, R.T., Smetacek, V., 1998. Biogeochemical controls and feedbacks on ocean primary production. Science 281, 200–206. https://doi.org/10.1126/science.281.5374.200.
Fernandes-Salvador, J.A., Davidson, K., Sourisseau, M., Revilla, M., Schmidt, W., Clarke, D., Miller, P.I., Arce, P., Fernández, R., Maman, L., Silva, A., Whyte, C., Mateo, M., Neira, P., Mateus, M., Ruiz-Villarreal, M., Ferrer, L., Silke, J., 2021. Current status of forecasting toxic harmful algae for the North-East Atlantic shellfish aquaculture industry. Front. Mar. Sci. 8, 666583 https://doi.org/10.3389/fmars.2021.666583.
Ferreira, A.S., Visser, A.W., MacKenzie, B.R., Payne, M.R., 2014. Accuracy and precision in the calculation of phenology metrics. J. Geophys. Res. Ocean. 119, 8438–8453. https://doi.org/10.1002/2014JC010323.
Ferreira, A., Garrido-Amador, P., Brito, A.C., 2019. Disentangling environmental drivers of phytoplankton biomass off Western Iberia. Front. Mar. Sci. 6, 1–17. https://doi.org/10.3389/fmars.2019.00044.

Ferreira, A., Brotas, V., Palma, C., Borges, C., Brito, A.C., 2021. Assessing phytoplankton bloom phenology in upwelling-influenced regions using ocean color remote sensing. Remote Sens 13, 1–27. https://doi.org/10.3390/rs13040675.
Fiúza, A.F.de G., de Macedo, M.E., Guerreiro, M.R., 1982. Climatological space and time variation of the Portuguese coastal upwelling. Oceanology 5, 31–40.
Fraga, S., Anderson, D.M., Bravo, I., Reguera, B., Steidinger, K.A., Yentsch, C.M., 1988. Influence of upwelling relaxation on dinoflagellates and shellfish toxicity in Ria de Vigo. Spain. Estuar. Coast. Shelf Sci. 27, 349–361. https://doi.org/10.1016/0272-7714(88)90093-5.
Franks, P.J.S., 2018. Recent Advances in Modelling of Harmful Algal Blooms. In: Glibert, P.M., Berdalet, E., Burford, M.A., Pitcher, G.C., Zhou, M. (Eds.), Global Ecology and Oceanography of Harmful Algal Blooms. Springer International Publishing, Cham, pp. 359–377. https://doi.org/10.1007/978-3-319-70069-4_19.
García-Lafuente, J., Delgado, J., Criado-Aldeanueva, F., Bruno, M., del Río, J., Vargas, J. M., 2006. Water mass circulation on the continental shelf of the Gulf of Cádiz. Deep. Res. Part II 53, 1182–1197. https://doi.org/10.1016/j.dsr2.2006.04.011.
García-Lafuente, J., Ruiz, J., 2007. The Gulf of Cádiz pelagic ecosystem: a review. Prog. Oceanogr. 74, 228–251. https://doi.org/10.1016/j.pocean.2007.04.001.
Garel, E., Laiz, I., Drago, T., Relvas, P., 2016. Characterisation of coastal counter-currents on the inner shelf of the Gulf of Cadiz. J. Mar. Syst. 155, 19–34. https://doi.org/10.1016/j.jmarsys.2015.11.001.
Gianella, F., Burrows, M.T., Swan, S.C., Turner, A.D., Davidson, K., 2021. Temporal and spatial patterns of harmful algae affecting Scottish shellfish aquaculture. Front. Mar. Sci. 8 https://doi.org/10.3389/fmars.2021.785174.
Giddings, S.N., MacCready, P., Hickey, B.M., Banas, N.S., Davis, K.A., Siedlecki, S.A., Trainer, V.L., Kudela, R.M., Pelland, N.A., Connolly, T.P., 2014. Hindcasts of potential harmful algal bloom transport pathways on the Pacific Northwest coast. J. Geophys. Res. Ocean 119, 2439–2461. https://doi.org/10.1002/2013JC009622.
Glibert, P.M., 2016. Margalef revisited: A new phytoplankton mandala incorporating twelve dimensions, including nutritional physiology. Harmful Algae 55, 25–30. https://doi.org/10.1016/j.hal.2016.01.008.
Glibert, P.M., 2020. Harmful algae at the complex nexus of eutrophication and climate change. Harmful Algae 91, 101583. https://doi.org/10.1016/j.hal.2019.03.001.
Glibert, P.M., Burford, M., 2017. Globally changing nutrient loads and harmful algal blooms: Recent advances, new paradigms, and continuing challenges. Oceanography 30, 58–69. http://www.jstor.org/stable/24897842.
Gobler, C.J., Sunda, W.G., 2012. Ecosystem disruptive algal blooms of the brown tide species, *Aureococcus anophagefferens* and *Aureoumbra lagunensis*. Harmful Algae 14, 36–45. https://doi.org/10.1016/j.hal.2011.10.013.
Gobler, C.J., Doherty, O.M., Hattenrath-Lehmann, T.K., Griffith, A.W., Kang, Y., Litaker, R.W., 2017. Ocean warming since 1982 has expanded the niche of toxic algal blooms in the North Atlantic and North Pacific oceans. Proc. Natl. Acad. Sci. 114 (19), 4975–4980. https://doi.org/10.1073/pnas.1619575114.
Goela, P., Danchenko, S., Icely, J.D., Lubian, L.M., Cristina, S., Newton, A., 2014. Using CHEMTAX to evaluate seasonal and interannual dynamics of the phytoplankton community off the South-west coast of Portugal. Estuar. Coast. Shelf Sci. 151, 112–123. https://doi.org/10.1016/j.ecss.2014.10.001.
Goela, P.C., Cordeiro, C., Danchenko, S., Icely, J., Cristina, S., Newton, A., 2016. Time series analysis of data for sea surface temperature and upwelling components from the southwest coast of Portugal. J. Mar. Syst. 163, 12–22. https://doi.org/10.1016/j.jmarsys.2016.06.002.
González Vilas, L., Spyrakos, E., Torres Palenzuela, J.M., Pazos, Y., 2014. Support Vector Machine-based method for predicting *Pseudo-nitzschia* spp. blooms in coastal waters (Galician rias. NW Spain). Prog. Oceanogr. 124, 66–77. https://doi.org/10.1016/j.pocean.2014.03.003.
Guallar, C., Delgado, M., Diogène, J., Fernández-Tejedor, M., 2016. Artificial neural network approach to population dynamics of harmful algal blooms in Alfacs Bay (NW Mediterranean): Case studies of *Karlodinium* and *Pseudo-nitzschia*. Ecol. Model. 338, 37–50. https://doi.org/10.1016/j.ecolmodel.2016.07.009.
Guallar, C., Cedric, B., Annie, C., 2017. Global and local factors driving the phenology of Alexandrium minutum (Halim) blooms and its toxicity. Harmful Algae 67, 44–60. https://doi.org/10.1016/j.hal.2017.05.005.
Hallegraeff, G.M., McCausland, M.A., Brown, R.K., 1995. Early warning of toxic dinoflagellate blooms of *Gymnodinium catenatum* in southern Tasmanian waters. J. Plankton Res. 17, 1163–1176. https://doi.org/10.1093/plankt/17.6.1163.
Hallegraeff, G.M., Blackburn, S.I., Doblin, M.A., Bolch, C.J.S., 2012. Global toxicology, ecophysiology and population relationships of the chain forming PST dinoflagellate *Gymnodinium catenatum*. Harmful Algae 14, 130–143. https://doi.org/10.1016/j.hal.2011.10.018.
Hallegraeff, G.M., Anderson, D.M., Belin, C., Bottein, M.-Y.D., Bresnan, E., Chinain, M., Enevoldsen, H., Iwataki, M., Karlson, B., McKenzie, C.H., Sunesen, I., Pitcher, G.C., Provoost, P., Richardson, A., Schweibold, L., Tester, P.A., Trainer, V.L., Yñiguez, A. T., Zingone, A., 2021a. Perceived global increase in algal blooms is attributable to intensified monitoring and emerging bloom impacts. Commun. Earth Environ. 2, 117. https://doi.org/10.1038/s43247-021-00178-8.
Hallegraeff, G., Enevoldsen, H., Zingone, A., 2021b. Global harmful algal bloom status reporting. Harmful Algae 102, 1–3. https://doi.org/10.1016/j.hal.2021.101992.
Hastie, T., Tibshirani, R., 1990. Exploring the nature of covariate effects in the proportional hazards model. Biometrics 46, 1005–1016. https://doi.org/10.2307/2532444.
Hickey, B., Geier, S., Kachel, N., MacFadyen, A., 2005. A bi-directional river plume: the Columbia in summer. Cont. Shelf Res. 25, 1631–1656. https://doi.org/10.1016/j.csr.2005.04.010.
Hickey, B.M., Trainer, V.L., Michael Kosro, P., Adams, N.G., Connolly, T.P., Kachel, N.B., Geier, S.L., 2013. A springtime source of toxic *Pseudo-nitzschia* cells on razor clam beaches in the Pacific Northwest. Harmful Algae 25, 1–14. https://doi.org/10.1016/j.hal.2013.01.006.
Hilbe, J.M., 2011. Negative binomial regression. Cambridge University Press.
Hoagland, P., Anderson, D.M., Kaoru, Y., White, A.W., 2002. The economic effects of harmful algal blooms in the United States: estimates, assessment issues, and information needs. Estuaries 25, 819–837. https://doi.org/10.1007/BF02804908.
Hoagland, P., Scatasta, S., 2006. The Economic Effects of Harmful Algal Blooms. In: Granéli, E., Turner, J.T. (Eds.), Ecology of Harmful Algae. Springer Berlin Heidelberg, Berlin, Heidelberg, pp. 391–402. https://doi.org/10.1007/978-3-540-32210-8_30.
Hugman, R., Stigter, T.Y., Monteiro, J.P., Costa, L., Nunes, L.M., 2015. Modeling the spatial and temporal distribution of coastal groundwater discharge for different water use scenarios under epistemic uncertainty: case study in South Portugal. Environ. Earth Sci. 73, 2657–2669. https://doi.org/10.1007/s12665-014-3709-4.
IPMA, 2013. Plano de ação Sistema Nacional de Monitorização de Moluscos Bivalves. Instituto Português do Mar e da Atmosfera, p. 16. I.P., novembro 2013.
Irwin, A.J., Finkel, Z.V, 2008. Mining a sea of data: deducing the environmental controls of ocean chlorophyll. PLoS One 3, 1–6. https://doi.org/10.1371/journal.pone.0003836.
Jeong, H.J., Yoo, Y.Du, Park, J.Y., Song, J.Y., Kim, S.T., Lee, S.H., Kim, K.Y., Won Ho, Yih, 2005. Feeding by phototrophic red-tide dinoflagellates: five species newly revealed and six species previously known to be mixotrophic. Aquat. Microb. Ecol. 40, 133–150. https://doi.org/10.3354/ame040133.
Karasiewicz, S., Lefebvre, A., 2022. Environmental Impact on Harmful Species *Pseudo-nitzschia* spp. and *Phaeocystis globosa* Phenology and Niche. J. Mar. Sci. Eng. 10, 174. https://doi.org/10.3390/jmse10020174.
Kirk, J.T.O., 1986. Light and Photosynthesis in Aquatic Ecosystems. Cambridge University Press, Cambridge.
Krug, L., Platt, T., Sathyendranath, S., Barbosa, A.B., 2017. Unravelling region-specific environmental drivers of phytoplankton across a complex marine domain (off SW Iberia). Remote Sens. Environ. 203, 162–184. https://doi.org/10.1016/j.rse.2017.05.029.
Krug, L.A., Platt, T., Barbosa, A.B., 2018a. Delineation of ocean surface provinces over a complex marine domain off SW Iberia: An objective abiotic-based approach. Reg. Stud. Mar. Sci. 18, 80–96. https://doi.org/10.1016/j.rsma.2018.01.003.
Krug, L., Platt, T., Sathyendranath, S., Barbosa, A.B., 2018b. Patterns and drivers of phytoplankton phenology off SW Iberia: A phenoregion based perspective. Prog. Oceanogr. 165, 233–256. https://doi.org/10.1016/j.pocean.2018.06.010.
Kudela, R.M., Berdalet, E., Bernard, S., Burford, M.A., Fernand, L.J., Lu, S., Roy, S., Tester, P.A., Usup, G., Magnien, R.E., Anderson, D.M., Cembella, A.D., Chinain, M., Hallegraeff, G.M., Reguera, B., Zingone, A., Enevoldsen, H., Urban, E., 2015. Harmful algal blooms: a scientific summary for policy makers. Harmful Algal Blooms. A Scientific Summary for Policy Maker. IOC/UNESCO 19. Paris (IOC/INF-1320).
Kudela, R.M., Hayashi, K., Caceres, C.G., 2020. Is San Francisco Bay resistant to *Pseudo-nitzschia* and domoic acid? Harmful Algae 92, 101617. https://doi.org/10.1016/j.hal.2019.05.010.
Lane, J.Q., Raimondi, P.T., Kudela, R.M., 2009. Development of a logistic regression model for the prediction of toxigenic *Pseudo-nitzschia* blooms in Monterey Bay, California. Mar. Ecol. Prog. Ser. 383, 37–51. https://doi.org/10.3354/meps07999.
Largier, J.L., 2020. Upwelling bays: how coastal upwelling controls circulation, habitat, and productivity in bays. Ann. Rev. Mar. Sci. 12, 415–447. https://doi.org/10.1146/annurev-marine-010419-011020.
Lelong, A., Hégaret, H., Soudant, P., Bates, S.S., 2012. *Pseudo-nitzschia* (Bacillariophyceae) species, domoic acid and amnesic shellfish poisoning: revisiting previous paradigms. Phycologia 51, 168–216. https://doi.org/10.2216/11-37.1.
Lewis, A.M., Coates, L.N., Turner, A.D., Percy, L., Lewis, J., 2018. A review of the global distribution of *Alexandrium minutum* (Dinophyceae) and comments on ecology and associated paralytic shellfish toxin profiles, with a focus on Northern Europe. J. Phycol. 54, 581–598. https://doi.org/10.1111/jpy.12768.
Llope, M., Chan, K.-S., Reid, P.C., Stige, L.C., Stenseth, N.C., 2009. Effects of environmental conditions on the seasonal distribution of phytoplankton biomass in the North Sea. Limnol. Oceanogr. 54, 512–524.
Lopez, C.B., Tilney, C.L., Muhlbach, E., Bouchard, J.N., Villac, M.C., Henschen, K.L., Markley, L.R., Abbe, S.K., Shankar, S., Shea, C.P., Flewelling, L., Garrett, M., Badylak, S., Phlips, E.J., Hall, L.M., Lasi, M.A., Parks, A.A., Paperno, R., Adams, D.H., Edwards, D.D., Schneider, J.E., Wald, K.B., Biddle, A.R., Landers, S.L., Hubbard, K. A., 2021. High-resolution spatiotemporal dynamics of harmful algae in the Indian River Lagoon (Florida)—a case study of *Aureoumbra lagunensis, Pyrodinium bahamense*, and *Pseudo-nitzschia*. Front. Mar. Sci. 8 https://doi.org/10.3389/fmars.2021.769877.
Loureiro, S., Newton, A., Icely, J.D., 2005. Microplankton composition, production and upwelling dynamics in Sagres (SW Portugal) during the summer of 2001. Sci. Mar. 69, 323–341.
Loureiro, S., Reñé, A., Garcés, E., Camp, J., Vaqué, D., 2011. Harmful algal blooms (HABs), dissolved organic matter (DOM), and planktonic microbial community dynamics at a near-shore and a harbour station influenced by upwelling (SW Iberian Peninsula). J. Sea Res. 65, 401–413. https://doi.org/10.1016/j.seares.2011.03.004.
Marañón, E., 2015. Cell size as a key determinant of phytoplankton metabolism and community structure. Ann. Rev. Mar. Sci. 7, 241–264. https://doi.org/10.1146/annurev-marine-010814-015955.
Marta-Almeida, M., Dubert, J., Peliz, Á., dos Santos, A., Queiroga, H., 2008. A modelling study of Norway lobster (*Nephrops norvegicus*) larval dispersal in southern Portugal: predictions of larval wastage and self-recruitment in the Algarve stock. Can. J. Fish. Aquat. Sci. 65, 2253–2268. https://doi.org/10.1139/F08-138.

Mateus, M., D. Silva, A., de Pablo, H., Moita, M.T., Quental, T., Pinto, L., 2013. Using Lagrangian elements to simulate alongshore transport of harmful algal blooms. Ocean Model. Coast. Manag. Stud. with MOHID 235–248.

Matus-Hernández, M.Á., Martínez-Rincón, R.O., Aviña-Hernández, R.J., Hernández-Saavedra, N.Y., 2019. Landsat-derived environmental factors to describe habitat preferences and spatiotemporal distribution of phytoplankton. Ecol. Model. 408, 108759 https://doi.org/10.1016/j.ecolmodel.2019.108759.

McCabe, R.M., Hickey, B.M., Kudela, R.M., Lefebvre, K.A., Adams, N.G., Bill, B.D., Gulland, F.M.D., Thomson, R.E., Cochlan, W.P., Trainer, V.L., 2016. An unprecedented coastwide toxic algal bloom linked to anomalous ocean conditions. Geophys. Res. Lett. 43 (10), 310–366. https://doi.org/10.1002/2016GL070023, 376.

McGillicuddy, D.J.J., Townsend, D.W., He, R., Keafer, B.A., Kleindinst, J.L., Li, Y., Manning, J.P., Mountain, D.G., Thomas, M.A., Anderson, D.M., 2011. Suppression of the 2010 *Alexandrium fundyense* bloom by changes in physical, biological, and chemical properties of the Gulf of Maine. Limnol. Oceanogr. 56, 2411–2426. https://doi.org/10.4319/lo.2011.56.6.2411.

McKenzie, C.H., Bates, S.S., Martin, J.L., Haigh, N., Howland, K.L., Lewis, N.I., Locke, A., Peña, A., Poulin, M., Rochon, A., Rourke, W.A., Scarratt, M.G., Starr, M., Wells, T., 2021. Three decades of Canadian marine harmful algal events: Phytoplankton and phycotoxins of concern to human and ecosystem health. Harmful Algae 102, 101852. https://doi.org/10.1016/j.hal.2020.101852.

Moita, M.T., 2001. Estrutura, variabilidade e dinâmica do fitoplâncton na Costa de Portugal Continental. University of Lisbon, Portugal, p. 272. Ph.D. Thesis.

Moita, M.T., Vilarinho, M.G., Palma, A.S., 1998. On the variability of *Gymnodinium catenatum* Graham blooms in Portuguese waters. In: Reguera, B., Blanco, J., Fernández, M.L., Wyatt, T. (Eds.), Harmful Microalgae. Xunta de Galicia and IOC of UNESCO, pp. 118–121.

Moita, M.T., Oliveira, P.B., Mendes, J.C., Palma, A.S., 2003. Distribution of chlorophyll a and *Gymnodinium catenatum* associated with coastal upwelling plumes off central Portugal. Acta Oecol. 24, S125–S132. https://doi.org/10.1016/S1146-609X(03)00011-0.

Moita, M., Sobrinho-Gonçalves, L., Oliveira, P., Palma, S., Falcão, M., 2006a. A bloom of *Dinophysis acuta* in a thin layer off North-West Portugal. African J. Mar. Sci. 28, 265–269. https://doi.org/10.2989/18142320609504160.

Moita, M.T., Palma, S., Oliveira, P.B., Vidal, T., Silva, A., Vilarinho, G., 2006b. The return of *Gymnodinium catenatum* after 10 years: bloom initiation and transport off the Portuguese coast. In: International Society for the Study of Harmful Algae 12th International Conference on Harmful Algae. Copenhagen, Denmark, 4-8 September 2006, p. 242.

Moita, M.T., Pazos, Y., Rocha, C., Nolasco, R., Oliveira, P.B., 2016. Toward predicting *Dinophysis* blooms off NW Iberia: a decade of events. Harmful Algae 53, 17–32. https://doi.org/10.1016/j.hal.2015.12.002.

Nielsen, L.T., Hansen, P.J., Krock, B., Vismann, B., 2016. Accumulation, transformation and breakdown of DSP toxins from the toxic dinoflagellate *Dinophysis acuta* in blue mussels, *Mytilus edulis*. Toxicon 117, 84–93. https://doi.org/10.1016/j.toxicon.2016.03.021.

Otero, J., Bode, A., Álvarez-salgado, X., Varela, M., 2018. Role of functional trait variability in the response of individual phytoplankton species to changing environmental conditions in a coastal upwelling zone. Mar. Ecol. Prog. Ser. 596, 33–47. https://doi.org/10.3354/meps12542.

Otto, S.A., Diekmann, R., Flinkman, J., Kornilovs, G., Mollmann, C., 2014. Habitat heterogeneity determines climate impact on zooplankton community structure and dynamics. PLoS One 9, 1–11. https://doi.org/10.1371/journal.pone.0090875.

Palenzuela, J.M., González Vilas, L., Bellas, F.M., Garet, E., González-Fernández, Á., Spyrakos, E., 2019. *Pseudo-nitzschia* blooms in a coastal upwelling system: remote sensing detection, toxicity and environmental variables. Water 11, 1954. https://doi.org/10.3390/w11091954.

Palma, S., Mouriño, H., Silva, A., Barão, M., Moita, T., 2010. Can *Pseudo-nitzschia* blooms be modeled by coastal upwelling in Lisbon Bay? Harmful Algae 9, 294–303. https://doi.org/10.1016/j.hal.2009.11.006.

Peliz, A., Santos, A.M.P., Oliveira, P.B., Dubert, J., 2004. Extreme cross-shelf transport induced by eddy interactions southwest of Iberia in winter 2001. Geophys. Res. Lett. 31, 1–4. https://doi.org/10.1029/2004GL019618.

Peliz, A., Dubert, J., Marchesiello, P., Teles-Machado, A., 2007. Surface circulation in the Gulf of Cadiz: model and mean flow structure. J. Geophys. Res. Ocean. 112 https://doi.org/10.1029/2007JC004159.

Peliz, A., Marchesiello, P., Santos, A.M.P., Dubert, J., Teles-Machado, A., Marta-Almeida, M., Le Cann, B., 2009. Surface circulation in the Gulf of Cadiz: 2. Inflow-outflow coupling and the Gulf of Cadiz slope current. J. Geophys. Res. Ocean. 114 https://doi.org/10.1029/2008JC004771.

Peperzak, L., Snoeijer, G.J., Dijkema, R., Gieskes, W.W.C., Joordens, J., Peeters, J.C.H., Schol, C., Vrieling, E.G., Zevenboom, W., 1996. Development of a *Dinophysis acuminata* bloom in the river rine plume (North Sea). In: Yasumoto, T., Oshima, Y., Fukuyo, Y. (Eds.), Harmful and Toxic Algal Blooms. United Nations Educational Scientific and Cultural Organization 7, Place of Fontenoy, Paris, pp. 273–276.

Piló, D., Barbosa, A.B., Teodósio, M.A., Encarnação, J., Leitão, F., Range, P., Krug, L.A., Cruz, J., Chícharo, L., 2018. Are submarine groundwater discharges affecting the structure and physiological status of rocky intertidal communities? Mar. Environ. Res. 136, 158–173. https://doi.org/10.1016/j.marenvres.2018.02.013.

Pinto, L., Mateus, M., Silva, A., 2016. Modelling the transport pathways of harmful algal blooms in the Iberian coast. Harmful Algae 53, 8–16. https://doi.org/10.1016/j.hal.2015.12.001.

Pires, R.F.T., Pan, M., Santos, A.M.P., Peliz, Á., Boutov, D., dos, Santos A., 2013. Modelling the variation in larval dispersal of estuarine and coastal ghost shrimp: *Upogebia congeners* in the Gulf of Cadiz. Mar. Ecol. Prog. Ser. 492, 153–168. https://doi.org/10.3354/meps10488.

Pires, R.F.T., Peliz, Á., Pan, M., dos Santos, A., 2020. There and back again" – how decapod megalopae find the way home: a modelling exercise for *Pachygrapsus marmoratus*. Prog. Oceanogr. 184, 102331 https://doi.org/10.1016/j.pocean.2020.102331.

Pitcher, G.C., Figueiras, F.G., Hickey, B.M., Moita, M.T., 2010. The physical oceanography of upwelling systems and the development of harmful algal blooms. Prog. Oceanogr. 85, 5–32. https://doi.org/10.1016/j.pocean.2010.02.002.

Pitcher, G.C., Jiménez, A.B., Kudela, R.M., Reguera, B., 2017. Harmful algal blooms in eastern boundary upwelling systems. Oceanography 30, 22–35. https://doi.org/10.5670/oceanog.2017.107.

Pitcher, G.C., Louw, D.C., 2021. Harmful algal blooms of the Benguela eastern boundary upwelling system. Harmful Algae 102, 101898. https://doi.org/10.1016/j.hal.2020.101898.

Prieto, L., Navarro, G., Rodríguez-Gálvez, S., Huertas, I.E., Naranjo, J.M., Ruiz, J., 2009. Oceanographic and meteorological forcing of the pelagic ecosystem on the Gulf of Cadiz shelf (SW Iberian Peninsula). Cont. Shelf Res. 29, 2122–2137. https://doi.org/10.1016/j.csr.2009.08.007.

R Core Team, 2020. R: A language and environment for statistical computing. R Foundation for Statistical Computing, Vienna, Austria http://www.R-project.org/ (accessed 08/01/2020).

Raine, R., McDermott, G., Silke, J., Lyons, K., Nolan, G., Cusack, C., 2010. A simple short range model for the prediction of harmful algal events in the bays of southwestern Ireland. J. Mar. Syst. 83, 150–157. https://doi.org/10.1016/j.jmarsys.2010.05.001.

Ralston, D.K., Moore, S.K., 2020. Modeling harmful algal blooms in a changing climate. Harmful Algae 91, 101729. https://doi.org/10.1016/j.hal.2019.101729.

Reguera, B., Bravo, I., Fraga, S., 1995. Autoecology and some life history stages of *Dinophysis acuta* Ehrenberg. J. Plankton Res. 17, 999–1015. https://doi.org/10.1093/plankt/17.5.999.

Reguera, B., Velo-Suárez, L., Raine, R., Park, M., 2012. Harmful *Dinophysis* species: a review. Harmful Algae 14, 87–106. https://doi.org/10.1016/j.hal.2011.10.016.

Relvas, P., Barton, E., 2002. Mesoscale patterns in the Cape São Vicente (Iberian Peninsula) upwelling region. J. Geophys. Res. 107, 1–23. https://doi.org/10.1029/2000JC000456.

Relvas, P., Barton, E.D., Dubert, J., Oliveira, P.B., Peliz, Á., da Silva, J.C.B., Santos, A.M.P., 2007. Physical oceanography of the western Iberia ecosystem: latest views and challenges. Prog. Oceanogr. 74, 149–173. https://doi.org/10.1016/j.pocean.2007.04.021.

Relvas, P., Luís, J., Santos, A.M.P., 2009. Importance of the mesoscale in the decadal changes observed in the northern Canary upwelling system. Geophys. Res. Lett. 36, L22601. https://doi.org/10.1029/2009GL040504.

Ribas-Ribas, M., Anfuso, E., Gómez-Parra, A., Forja, J.M., 2013. Tidal and seasonal carbon and nutrient dynamics of the Guadalquivir estuary and the Bay of Cádiz (SW Iberian Peninsula). Biogeosciences 10, 4481–4491. https://doi.org/10.5194/bg-10-4481-2013.

Roberts, S.D., Van Ruth, P.D., Wilkinson, C., Bastianello, S.S., Bansemer, M.S., 2019. Marine heatwave, harmful algae blooms and an extensive fish kill event during 2013 in South Australia. Front. Mar. Sci. 6 https://doi.org/10.3389/fmars.2019.00610.

Robinson, I.S., 2010. Discovering the Ocean from Space: The unique applications of satellite oceanography. Springer Science & Business Media.

Rochford, P.A., Kara, A.B., Wallcraft, A.J., Arnone, R.A., 2001. Importance of solar subsurface heating in ocean general circulation models. J. Geophys. Res. Ocean. 106, 30923–30938. https://doi.org/10.1029/2000JC000355.

Rossini, G.P., 2014. Toxins and Biologically Active Compounds from Microalgae. Volume 2 Biological Effects and Risk Management, 1st ed. CRC Press. https://doi.org/10.1201/b16806.

Ruiz-Villarreal, M., García-García, L.M., Cobas, M., Díaz, P.A., Reguera, B., 2016. Modelling the hydrodynamic conditions associated with *Dinophysis* blooms in Galicia (NW Spain). Harmful Algae 53, 40–52. https://doi.org/10.1016/j.hal.2015.12.003.

Ryan, J.P., Kudela, R.M., Birch, J.M., Blum, M., Bowers, H.A., Chavez, F.P., Doucette, G.J., Hayashi, K., Marin III, R., Mikulski, C.M., Pennington, J.T., Scholin, C.A., Smith, G.J., Woods, A., Zhang, Y., 2017. Causality of an extreme harmful algal bloom in Monterey Bay, California, during the 2014–2016 northeast Pacific warm anomaly. Geophys. Res. Lett. 44, 5571–5579. https://doi.org/10.1002/2017GL072637.

Sánchez, R.F., Relvas, P., Martinho, A., Miller, P., 2008. Physical description of an upwelling filament west of Cape St. Vincent in late October 2004. J. Geophys. Res. Oceans 113. https://doi.org/10.1029/2007JC004430.

Sañé, E., Valente, A., Fatela, F., Cabral, M.C., Beltrán, C., Drago, T., 2019. Assessment of sedimentary pigments and phytoplankton determined by CHEMTAX analysis as biomarkers of unusual upwelling conditions in summer 2014 off the SE coast of Algarve. J. Sea Res. 146, 33–45. https://doi.org/10.1016/j.seares.2019.01.007.

Sanseverino, I., Conduto António, D., Pozzoli, L., Dobricic, S., Lettieri, T., 2016. Algal bloom and its economic impact, EUR 27905. Publications Office of the European Union, Luxembourg, p. 48. https://doi.org/10.2788/660478.

Santos, M., Mouriño, H., Moita, M.T., Silva, A., Amorim, A., Oliveira, P.B., 2020. Characterizing phytoplankton biomass seasonal cycles in two NE Atlantic coastal bays. Cont. Shelf Res. 207, 104200 https://doi.org/10.1016/j.csr.2020.104200.

Santos, M., Moita, M.T., Oliveira, P.B., Amorim, A., 2021. Phytoplankton communities in two wide-open bays in the Iberian upwelling system. J. Sea Res. 167, 101982 https://doi.org/10.1016/j.seares.2020.101982.

Sathyendranath, S., Brewin, R.J.W., Brockmann, C., Brotas, V., Calton, B., Chuprin, A., Cipollini, P., Couto, A.B., Dingle, J., Doerffer, R., Donlon, C., Dowell, M., Farman, A., Grant, M., Groom, S., Horseman, A., Jackson, T., Krasemann, H., Lavender, S., Martinez-Vicente, V., Mazeran, C., Mélin, F., Moore, T.S., Müller, D., Regner, P.,

Roy, S., Steele, C.J., Steinmetz, F., Swinton, J., Taberner, M., Thompson, A., Valente, A., Zühlke, M., Brando, V.E., Feng, H., Feldman, G., Franz, B.A., Frouin, R., Gould, R.W., Hooker, S.B., Kahru, M., Kratzer, S., Mitchell, B.G., Muller-Karger, F.E., Sosik, H.M., Voss, K.J., Werdell, J., Platt, T., 2019. An ocean-colour time series for use in climate studies: the experience of the ocean-colour climate change initiative (OC-CCI). Sensors 19 (19), 4285. https://doi.org/10.3390/s19194285.

Seegers, B.N., Birch, J.M., Marin III, R., Scholin, C.A., Caron, D.A., Seubert, E.L., Howard, M.D.A., Robertson, G.L., Jones, B.H., 2015. Subsurface seeding of surface harmful algal blooms observed through the integration of autonomous gliders, moored environmental sample processors, and satellite remote sensing in southern California. Limnol. Oceanogr. 60, 754–764. https://doi.org/10.1002/lno.10082.

Shumway, S.E., Burkholder, J.M., Morton, S.L., 2018. Harmful algal blooms: a compendium desk reference. John Wiley & Sons.

Siegel, D.A., Doney, S.C., Yoder, J.A., 2002. The North Atlantic spring phytoplankton bloom and Sverdrup's critical depth hypothesis. Science 296, 730–733. https://doi.org/10.1126/science.1069174.

Silva, A., Palma, S., Oliveira, P.B., Moita, M.T., 2009. Composition and interannual variability of phytoplankton in a coastal upwelling region (Lisbon Bay, Portugal). J. Sea Res. 62, 238–249. https://doi.org/10.1016/j.seares.2009.05.001.

Silva, A., Pinto, L., Rodrigues, S.M., Pablo, H.de, Santos, M., Moita, T., Mateus, M., 2016. A HAB warning system for shellfish harvesting in Portugal. Harmful Algae 53, 33–39. https://doi.org/10.1016/j.hal.2015.11.017.

Singh, A., Hårding, K., Reddy, H.R.V, Godhe, A., 2014. An assessment of *Dinophysis* blooms in the coastal Arabian Sea. Harmful Algae 34, 29–35. https://doi.org/10.1016/j.hal.2014.02.006.

Smayda, T.J., 2010. Adaptations and selection of harmful and other dinoflagellate species in upwelling systems. 2. Motility and migratory behaviour. Prog. Oceanogr. 85, 71–91. https://doi.org/10.1016/j.pocean.2010.02.005.

Smayda, T.J., Reynolds, C.S., 2001. Community Assembly in marine phytoplankton: application of recent models to harmful dinoflagellate blooms. J. Plankton Res. 23, 447–461. https://doi.org/10.1093/plankt/23.5.447.

Smayda, T., Trainer, V., 2010. Dinoflagellate blooms in upwelling systems: seeding, variability, and contrasts with diatom bloom behaviour. Prog. Oceanogr. 85, 92–107. https://doi.org/10.1016/j.pocean.2010.02.006.

Smith, J., Connell, P., Evans, R.H., Gellene, A.G., Howard, M.D.A., Jones, B.H., Kaveggia, S., Palmer, L., Schnetzer, A., Seegers, B.N., Seubert, E.L., Tatters, A.O., Caron, D.A., 2018. A decade and a half of *Pseudo-nitzschia* spp. and domoic acid along the coast of southern California. Harmful Algae 79, 87–104. https://doi.org/10.1016/j.hal.2018.07.007.

Sordo, I., Barton, E.D., Cotos, J.M., Pazos, Y., 2001. An inshore Poleward current in the NW of the Iberian Peninsula detected from satellite images, and its relation with *G. catenatum* and *D. acuminata* Blooms in the Galician Rias. Estuar. Coast. Shelf Sci. 53, 787–799. https://doi.org/10.1006/ecss.2000.0788.

Stumpf, R.P., Tomlinson, M.C., Calkins, J.A., Kirkpatrick, B., Fisher, K., Nierenberg, K., Currier, R., Wynne, T.T., 2009. Skill assessment for an operational algal bloom forecast system. J. Mar. Syst. 76, 151–161. https://doi.org/10.1016/j.jmarsys.2008.05.016.

Sverdrup, H.U., 1953. On conditions for the vernal blooming of phytoplankton. ICES J. Mar. Sci. 18, 287–295. https://doi.org/10.1093/icesjms/18.3.287.

Thackeray, S.J., Jones, I.D., Maberly, S.C., 2008. Long-term change in the phenology of spring phytoplankton: species-specific responses to nutrient enrichment and climatic change. J. Ecol. 96, 523–535. https://doi.org/10.1111/j.1365-2745.2008.01355.x.

Tilstone, G.H., Figueiras, F.G., Fraga, F., 1994. Upwelling-downwelling sequences in the generation of red tides in a coastal upwelling system. Mar. Ecol. Prog. Ser. 112 (3), 241–253.

Trainer, V.L., Pitcher, G.C., Reguera, B., Smayda, T.J., 2010. The distribution and impacts of harmful algal bloom species in eastern boundary upwelling systems. Prog. Oceanogr. 85, 33–52. https://doi.org/10.1016/j.pocean.2010.02.003.

Trainer, V.L., Bates, S.S., Lundholm, N., Thessen, A.E., Cochlan, W.P., Adams, N.G., Trick, C.G., 2012. *Pseudo-nitzschia* physiological ecology, phylogeny, toxicity, monitoring and impacts on ecosystem health. Harmful Algae 14, 271–300. https://doi.org/10.1016/j.hal.2011.10.025.

Trainer, V.L., 2020. GlobalHAB: Evaluating, Reducing and Mitigating the Cost of Harmful Algal Blooms: A Compendium of Case Studies. North Pacific Marine Science Organization, Victoria, BC, Canada, p. 107. https://doi.org/10.25607/OBP-1709 (PICES Scientific Report No. 59)https://doi.org/.

Trainer, V.L., Moore, S.K., Hallegraeff, G., Kudela, R.M., Clement, A., Mardones, J.I., Cochlan, W.P., 2020a. Pelagic harmful algal blooms and climate change: Lessons from nature's experiments with extremes. Harmful Algae 91, 1–14. https://doi.org/10.1016/j.hal.2019.03.009.

Trainer, V.L., Kudela, R.M., Hunter, M.V, Adams, N.G., McCabe, R.M., 2020b. Climate Extreme Seeds a New Domoic Acid Hotspot on the US West Coast. Front. Clim. 2 https://doi.org/10.3389/fclim.2020.571836.

Vale, P., 2013. Can solar/geomagnetic activity restrict the occurrence of some shellfish poisoning outbreaks? The example of PSP caused by *Gymnodinium catenatum* at the Atlantic Portuguese coast. Biophysics (Oxf) 58, 554–567. https://doi.org/10.1134/S0006350913040179.

Vale, P., de, M., Sampayo, M.A., 2003. Seasonality of diarrhetic shellfish poisoning at a coastal lagoon in Portugal: rainfall patterns and folk wisdom. Toxicon 41, 187–197. https://doi.org/10.1016/S0041-0101(02)00276-3.

Vale, P., Botelho, M.J., Rodrigues, S.M., Gomes, S.S., de, M., Sampayo, M.A., 2008. Two decades of marine biotoxin monitoring in bivalves from Portugal (1986–2006): A review of exposure assessment. In: Harmful Algae, 7, pp. 11–25. https://doi.org/10.1016/j.hal.2007.05.002.

Velo-Suárez, L., González-Gil, S., Pazos, Y., Reguera, B., 2014. The growth season of *Dinophysis acuminata* in an upwelling system embayment: A conceptual model based on in situ measurements. Deep Sea Res. Part II Top. Stud. Oceanogr. 101, 141–151. https://doi.org/10.1016/j.dsr2.2013.03.033.

Vidal, T., Calado, A.J., Moita, M.T., Cunha, M.R., 2017. Phytoplankton dynamics in relation to seasonal variability and upwelling and relaxation patterns at the mouth of Ria de Aveiro (West Iberian Margin) over a four-year period. PLoS One 1–25. https://doi.org/10.1371/journal.pone.0177237.

Weithoff, G., Beisner, B.E., 2019. Measures and approaches in trait-based phytoplankton community ecology – from freshwater to marine ecosystems. Front. Mar. Sci. https://doi.org/10.3389/fmars.2019.00040.

Wells, M.L., Trainer, V.L., Smayda, T.J., Karlson, B.S.O., Trick, C.G., Kudela, R.M., Ishikawa, A., Bernard, S., Wulff, A., Anderson, D.M., Cochlan, W.P., 2015. Harmful algal blooms and climate change: learning from the past and present to forecast the future. Harmful Algae 49, 68–93. https://doi.org/10.1016/j.hal.2015.07.009.

Wells, M.L., Karlson, B., Wulff, A., Kudela, R., Trick, C., Asnaghi, V., Berdalet, E., Cochlan, W., Davidson, K., De Rijcke, M., Dutkiewicz, S., Hallegraeff, G., Flynn, K.J., Legrand, C., Paerl, H., Silke, J., Suikkanen, S., Thompson, P., Trainer, V.L., 2020. Future HAB science: Directions and challenges in a changing climate. Harmful Algae 91, 101632. https://doi.org/10.1016/j.hal.2019.101632.

Wood, S.N., 2017. Generalized additive models: an introduction with R. CRC press.

Zarauz, L., Irigoien, X., Urtizberea, A., Gonzalez, M., 2007. Mapping plankton distribution in the Bay of Biscay during three consecutive spring surveys. Mar. Ecol. Prog. Ser. 345, 27–39. https://doi.org/10.3354/meps06970.

Zhang, H.-M., Bates, J., Reynolds, R., 2006. Assessment of composite global sampling: sea surface wind speed. Geophys. Res. Lett. 33, 1–5. https://doi.org/10.1029/2006GL027086.

Zhu, Z., Qu, P., Fu, F., Tennenbaum, N., Tatters, A.O., Hutchins, D.A., 2017. Understanding the blob bloom: Warming increases toxicity and abundance of the harmful bloom diatom *Pseudo-nitzschia* in California coastal waters. Harmful Algae 67, 36–43. https://doi.org/10.1016/j.hal.2017.06.004.

Zuur, A.F., 2012. A beginner's guide to generalized additive models with R. Highland Statistics Limited, Newburgh, NY, USA, pp. 1–206.

Zuur, A.F., Ieno, E.N., Walker, N.J., Saveliev, A.A., Smith, G.M., 2009. Mixed effects models and extensions in ecology with R. Springer, New York (Vol. 574).